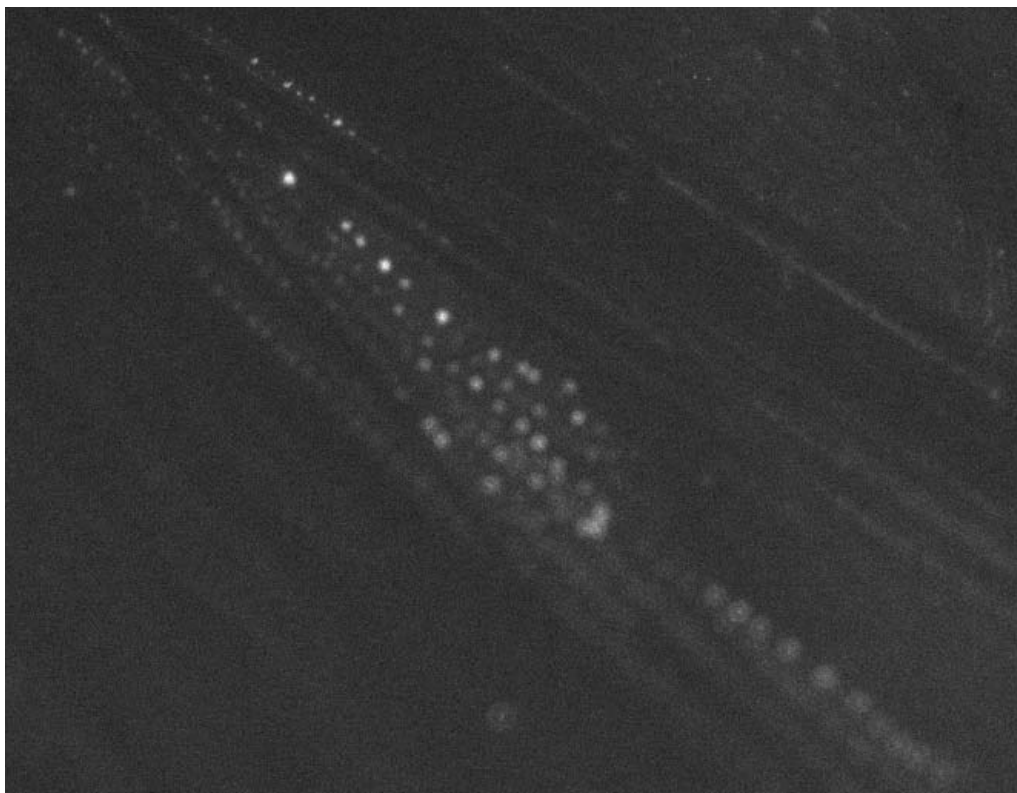


Structural transition of DMPG during phase transition: A thermodynamic study



Bachelor Thesis by

Morten Møller

Supervisor

Prof. Thomas Heimburg

Biomembrane Biophysics Group at the
Niels Bohr institute, University of Copenhagen, Denmark

12 June, 2009

Resume

Det negativt ladede phospholipid dimyristoyl phosphatidylglycerol (DMPG) har en meget besynderlig faseovergang ved en pH over 6 og en NaCl concentration under 100 mM. Phaseovergangen for DMPG identificeres ved en bred faseovergang med tre kalorimetriske peaks, der menes at være en intermediær fase mellem to vesicle konfigurationer. Faseovergangen besidder specielle fysiske egenskaber såsom øget viscositet, øget ledningsvne og større gennemsigtighed. Der findes flere teorier for dens struktur, men ingen virker fyldestgørende tallet være modstridende eksperimentelle beviser. Et vigtigt punkt er at visse teorier underbygger at vesikel strukturen bevares under faseovergangen mens andre teorier påstår det modsatte.

I denne bachelor thesis undersøges gennem kalorimetriske, rheologiske og fluorescerende mikroskopi målinger faseovergangens afhængighed af bevarelsen af vesiclerne samt den negative ladnings betydning for faseovergangen. Resultaterne viser at faseovergangen afhænger kun i lille grad af vesikel størrelsen, hvilket stemmer overens med teorien om dannelsen af netværk mellem vesiklerne i faseovergangen. Envidere vises det at denne intermediære fase afhænger af den negative ladning og at den intermediære fase eksisterer over hele faseovergangen.

Contents

Introduction and motivation	3
Theory.....	4
2.1 Lipids and membranes.....	4
2.2 Phase behavior.....	5
2.1.1 Phase transition.....	5
2.1.2 Ionic strength and pH dependence.....	6
2.3 Mechanical properties.....	7
2.4 DMPG phase behavior	9
2.4.1 Facts.....	9
2.4.2 Theories	10
Materials and Methods	11
3.1 Chemicals and samples.....	11
3.2 Vesicle preparation.....	11
3.2.2 Sonication.....	11
3.2.1 Extrusion.....	12
3.2.3 Evaporation.....	12
3.3 Viscosity	13
3.4 Differential Scanning Calorimetry	13
3.4.1 Principles	13
3.4.2 Experiment	14
3.5 Fluorescence microscopy	14
Data analysis	15
4.1 Rheology.....	15
4.2 Differential scanning calorimetry	15
Results.....	16
5.1 pH and NaCl dependence	16

5.1.1 DSC profiles	16
5.1.2 Viscosity profiles.....	19
5.2 Vesicle sizes	21
5.2.1 DSC profiles.....	21
5.2.2 Viscosity profiles.....	23
5.3 Area expansion.....	25
5.4 Bending modulus.....	26
5.5 Fluorescence Microscopy	27
Discussion	28
6.1 pH and ionic dependence.....	28
6.1.1 DSC profiles	28
6.1.2 Viscosity curves.....	28
6.1.3 Heat capacity and viscosity curves compared	29
6.2 Vesicle sizes	30
6.2.1 Viscosity	30
6.2.2 DSC profiles	30
6.3 Fluorescence microscopy	31
Errors	32
Conclusion	33
References	34
Appendix A	36
A.1 Enthalpy change for phase transition.....	36
A.2 Highest viscosity change	37
A.3 Influence of Dye	38

Introduction and motivation

Many biological functions involve the cell and intracellular membranes, examples are nerve pulse propagation, virus fusion, endo- or exocytosis. To understand these functions and their regulation a better understanding of biological membranes on the molecular level is crucial. One particular interest is the negatively charged lipid dimyristoyl phosphatidylglycerol (DMPG) which exhibits, at ionic strength below 100 nm and a pH value above 6, a number of so far not well understood properties. It shows a complex melting behavior over a wide temperature region that is combined with changes in the viscosity, conductivity and light scattering events. This phase behavior is of biological relevance because it occurs at physiological temperatures and it is possible that cells or viruses use similar concepts to trigger structural changes in their membranes.

The goal of this thesis is to examine what structural events occur through the use of differential scanning calorimetry, rheology and fluorescence microscopy. It is likely that the observed changes are due to the combination of a charged headgroup and a short hydrophobic tail, hence varying the pH and ionic strength should tell something about the phase behavior. To get an inside of the structural phenomena vesicles of different sizes will be prepared to learn more about the relation between the total lipid concentration and the surface area of the membrane. This is of particular importance because it will help elucidate between conflicting theories about the structural events.

Theory

2.1 Lipids and membranes

Lipids can have both aliphatic (open chain) and ring-formed structures and they can vary depending on headgroup sizes, charges and chain lengths making them the chemically most diverse group of molecules in cells. Membrane lipids consist of four classes: phospholipids, glycolipids, sphingolipids and sterols where phospholipids are the most abundant. They have a hydrophilic headgroup and a hydrophobic tail. The tail is composed of two hydrocarbon chains (that are not necessarily identical), bound to a glycerol molecule that itself is bound to the headgroup through a phosphodiester bond. The phospholipids can be divided into several subclasses depending on which derivatives are attached as the polar headgroup. The most important classes for eukaryotic membranes are: diacylglycerol-phosphatidylethanolamine (PE), diacylglycerol-phosphatidylcholine (PC), diacylglycerol-phosphatidylserine (PS), diacylglycerol-phosphatidylglycerol (PG), diacylglycerol-phosphatidylinositol (PI) and diacylglycerol-phosphatidic acid (PA). Most phospholipids are negatively charged, while some are neutral in total charge because they are zwitterionic. The study of the properties of charged lipids is therefore of high biological significance. [1]

Phospholipids are amphiphatic molecules (contains both hydrophobic and hydrophilic groups) that tend to self-assemble in an aqueous environment to spontaneously form different structures. The most common structures are lamellar, hexagonal and cubic phases. The propensity of the hydrophobic moieties to self-associate (entropically driven by water), and the tendency of the hydrophilic moieties to interact with aqueous environments and with each other, is the physical basis of the spontaneous formation of membranes. This same principle is occurring within the cell to produce organelles. In addition to barrier function, lipids provide membranes with the potential for budding, fission and fusion, characteristics that are essential for cell division and intracellular trafficking. [1,2]

The lipid bilayer consists of a hydrophobic and a hydrophilic portion. The hydrocarbon core consists of aliphatic lipid chains and is roughly 30 Å wide in a typical bilayer. The interfacial region of the bilayer comprises the lipid headgroups and is quite large, roughly 15 Å across.

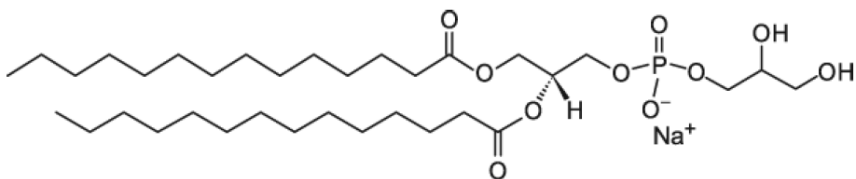


Figure 1: Molecular structure of DMPG. [3]

The phase behavior of 1,2-dimyristoyl-*sn*-glycero-3-phosphoglycerol (DMPG) will be studied which belongs to the PG phospholipid class. It contains two identical and saturated fatty acyl chains of 14 C atoms in length and is negatively charged. It exhibits an unusual broad phase transition at low salt concentrations and at above pH 5. The structures they form are in the phase transition are still unknown.

2.2 Phase behavior

Lipids can adopt various phases, which are characterized by a different spatial arrangement and motional freedom of each lipid with respect to its neighbor. In other words a phase reflects the systems degree of order. The lipid bilayer can assume different states depending on the temperature. The number and type of possible phase states of lipids varies depending on the lipid. The phases of the bilayer membranes are:

L_c: crystalline or “native” phase.

L_{β'}: solid ordered or “gel” phase. The lipid chains are packed highly ordered and tilted.

P_{β'}: “ripple” phase. Lipids are in highly ordered state but shows line defects.

L_α: liquid disordered or “fluid” phase. Lipid chains are disordered and distributed randomly in the membrane. [4]

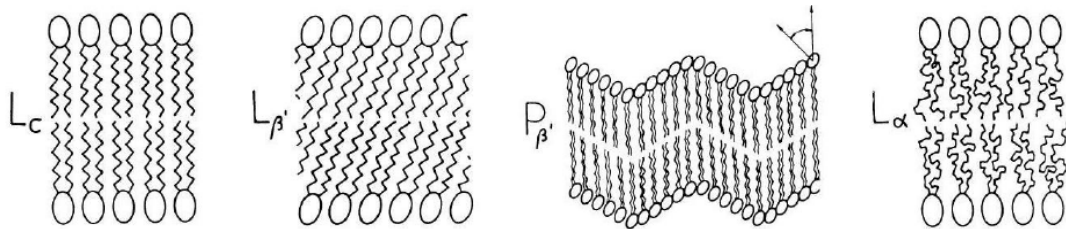


Figure 2.1: Different lipid phases. From the left: crystalline, gel, ripple and fluid phases. Adapted from [4]

2.1.1 Phase transition

As the membrane changes from the gel to the fluid state the thickness of the bilayer decreases and the packing area of the lipids increase as the acyl chains of the lipids become disordered. The packing area is increased by 25% while the volume expands by 4%. [5]

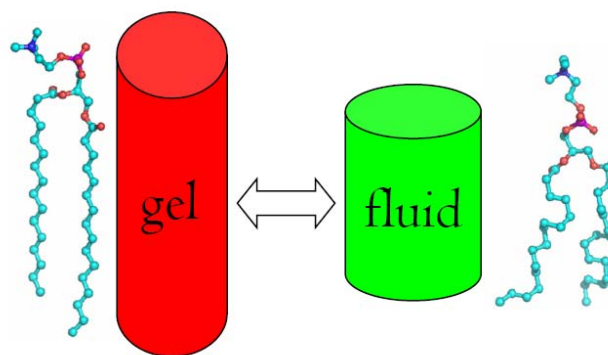


Figure 2.2: Schematic of phospholipid as it goes through from trans (ordered) to gauche (disordered) isomerization. The overall packaging area increases and their structure becomes more fluid. [6]

The most important structural change in the main phase transition is the conformational change of the acyl chain, involving the rotational isomerization (trans/ordered → gauche/disordered) of the

acyl chains. Increasing the disorder is the driving force for the chain melting transition and causes the the lipid to go from an ordered to a disordered state. This results in a loosening of the molecular packaging which decrease the bilayer thickness and increase the average cross-sectional area of the phospholipids within the bilayer. [7]

2.1.2 Ionic strength and pH dependence

The main property of the headgroups of lipids is their polarity, resulting in their solubility in water. When dealing with charged surfaces hydration forces can be neglected since these forces interact at short distances. [8] Importantly, the headgroup size has little effect on the transition temperature. Rather, it is the electrostatic charge of the headgroup which is important. Most naturally occurring lipids are charged including DMPG which has a negative charge at neutral pH. As mentioned earlier the fluid state has a packing area that is larger than that of the gel phase. Because electrostatic interactions decrease with distance the interactions are larger in the gel phase. The mutual repulsion of the negatively charged groups favors expansion of the membrane so that the transition temperature is lowered by an amount proportional to the charge density and raised proportional to the expansion of the molecular packing area at the phase transition. [6] This leads to the conclusion that lowering the net charge increases the stability of the gel phase relative to the fluid phase which increases the transition temperature. A formula has been derived known as the Gouy-Chapman theory for the shift in transition temperature going from gel to fluid phase.

$$\Delta T_t = \frac{-2kT}{\epsilon} \frac{N_A}{4S} \sigma \Delta A + \frac{e}{\pi} \left(\frac{k_B T}{\epsilon} \right)^2 \frac{N_A}{4S} \kappa \Delta A \quad (2.1)$$

Here ϵ is the dielectric constant, ΔS the change in entropy, e the elementary charge, k_B the Boltzmann constant and κ is a function for the thickness of the membrane and is proportional to the salt concentration. [9] The essential parameters are the charge density σ , the salt dependence and the change in the area per molecule ΔA at the transition. The first term in the equation shows a linear decrease in the transition temperature with increasing charge density while the second term shows an increase in the transition temperature with increasing salt concentration.

The presence of ions in the solution other than the charged lipids affects the thermal behavior of lipids because the ions affect the membrane potential by shielding the charges of the membrane. Figure 2.3 shows the effects of temperature, pH and added NaCl (n_m) to most lipids.

The degree of dissociation is the fraction of the lipids carrying a negative charge and is proportional to the charge density.. Increasing the ionic strength increases the degree of dissociation, resulting in a lowering of transition temperature. Thus increasing salt concentration can have one of two effects: it will fluidize the membrane at intermediate to high temperature and high pH while condensing the membrane at lower temperature and at lower pH. For which of these two tendencies will occur, depends on the degree of dissociation.

Increasing pH causes an increase in the ionization of the lipids. This increases the charge repulsion between the lipids thus increasing the degree of dissociation.

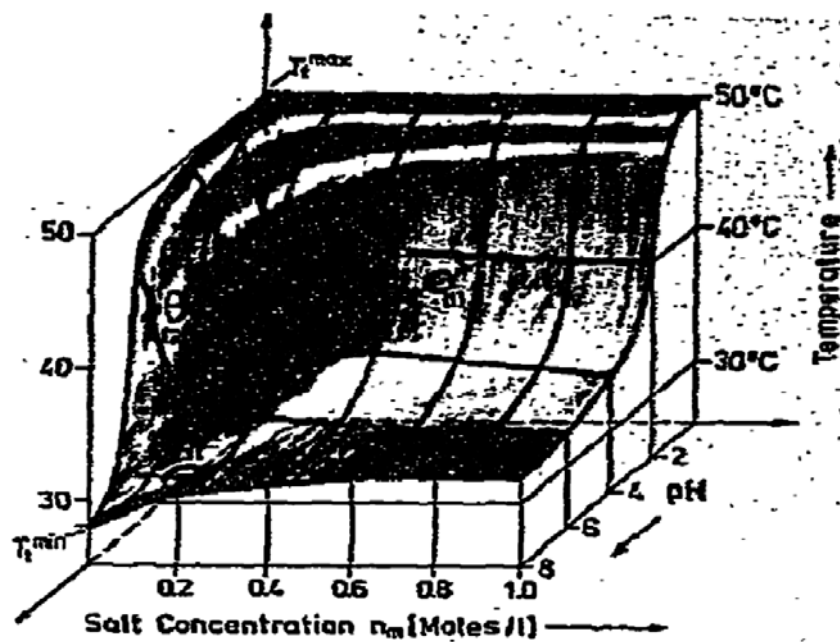


Figure 2.3: Effect of pH and salt (NaCl) on the transition temperature on lipids. As can be seen at low pH the highest transition temperature is found. At intermediate pH, increasing salt concentration lowers the transition temperature while at high pH the transition temperature increases. For almost any salt concentration, increasing the pH lowers the gel → fluid transition. [9]

2.3 Mechanical properties

Membranes can be regarded as thin elastic sheets that can be described in terms of their in-plane elasticity and bending. Lipid bilayers respond elastically to mechanical deformations which include bending, stretching or compression of the membrane but have little resistance to shear. [10]

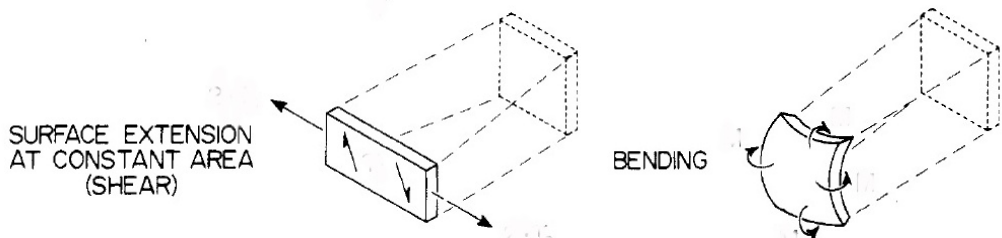


Figure 2.3: Types of deformation. The area compressibility (left), and at the bending modulus (right). Adapted from [11]

As mentioned before significant changes in both volume and area of the individual molecules occur in the melting region. From previous work [12] it has been shown that the volume and area compressibilities, as well as bending elasticities of membranes can be described as functions of the heat capacity. In this study the volume compressibilities as well as the thickness expansion coefficient will be ignored. The change in membrane area is proportional to the enthalpy changes and therefore the excess area compressibility can be expressed in relation to the heat capacity as:

$$\Delta \kappa_T^{\text{area}} = \frac{V_{\text{area}} T}{\Delta C_p} \Delta \epsilon_T \quad (2.2)$$

where ΔC_p is the excess heat capacity, $\gamma_{\text{Area}} = 8.93 \cdot 10^3 \text{ cm}^2/\text{J}$ is a proportionality factor and the area $\langle A \rangle = 2.21 \cdot 10^6 \text{ cm}^2/\text{g}$ has been calculated a mean between that of the gel and fluid phase. (These values are for DPPC and are assumed to be similar for DMPG). It can be seen that the lateral excess compressibility is linked to fluctuations in the membrane. The area compressibility at a specific temperature can be obtained by:

$$\kappa_T^{\text{Area}}(T) = \kappa_{T,0}^{\text{Area}} + \Delta \kappa_T^{\text{Area}}(T) \quad (2.3)$$

In the phase transition a fraction of the lipids become fluid and the area compressibility can be approximated by:

$$\kappa_T^{\text{Area}}(T) = (1 - f) \kappa_{T,0}^{\text{Area, gel}} + f \kappa_{T,0}^{\text{Area, fluid}} + \frac{\gamma_{\text{Area}} T}{\langle A \rangle} \Delta C_p \quad (2.4)$$

Where f is the fractional degree of melting and is defined to be proportional to the excess heat at a given temperature by the following relation:

$$f = \frac{\int_{T_1}^T C_p(T) dT}{\int_{T_1}^{T_2} C_p(T) dT} \quad (2.5)$$

where T_1 is the temperature at the beginning of the phase transition and T_2 is the temperature at the end of the phase transition. It has been demonstrated [12] that differences in headgroups do not have large influence on the bending modulus. The constants for DMPG can therefore be approximated for those for DMPC. ($\kappa_{T,0}^{\text{Area, gel}} = 1 \cdot 10^4 \text{ cm}^2/\text{J}$ and $\kappa_{T,0}^{\text{Area, fluid}} = 6.9 \cdot 10^4 \text{ cm}^2/\text{J}$. [12]

From the enthalpy change the bending modulus of the membrane at the phase transition can be calculated.. This can be used to find the bending elasticity:

$$\kappa_b = \kappa_{b,0} + \frac{16 \gamma_{\text{Area}}^2 T}{D^2 \langle A \rangle} \Delta C_p \quad (2.6)$$

where $D = 35.3 \text{ \AA}$ is the thickness of the membrane. The bending modulus $K_B = 1/\kappa_b$ is the inverse of the bending elasticity. [12]

2.4 DMPG phase behavior

2.4.1 Facts

The transition region narrows with increasing salt concentration until it reaches a single peak at 23°C at 100 mM NaCl. Here the negative charge of DMPG is shielded and it shows a thermal behavior similar to DMPC. The similarity is due to the two lipids having an almost identical structure. Only the headgroups are different. However in salt concentrations lower than 100 mM NaCl, DMPG shows a very complex and wide gel-fluid phase transition spanning 18 – 35°C depending on salt concentration and the pH. This is due to the neutralization of the charged headgroups which stabilizes the highly packed gel phase. This shows that the phase transition of interest is dependent on the presence of charged headgroups. [14, 15] It has been shown that large faceted vesicles below the phase transition and smaller, mostly spherical vesicles above the phase transition exist. [16, 17] The structure(s) within the phase transition remains unknown.

In the phase transition there is a sharp decrease in light scattering [14] (higher transparency) at the first transition peak, followed by sharp increase at the end of the phase transition. In addition, the viscosity increased considerably in correlation with the DSC profiles. The phase transition also exhibits an increase in conductivity.

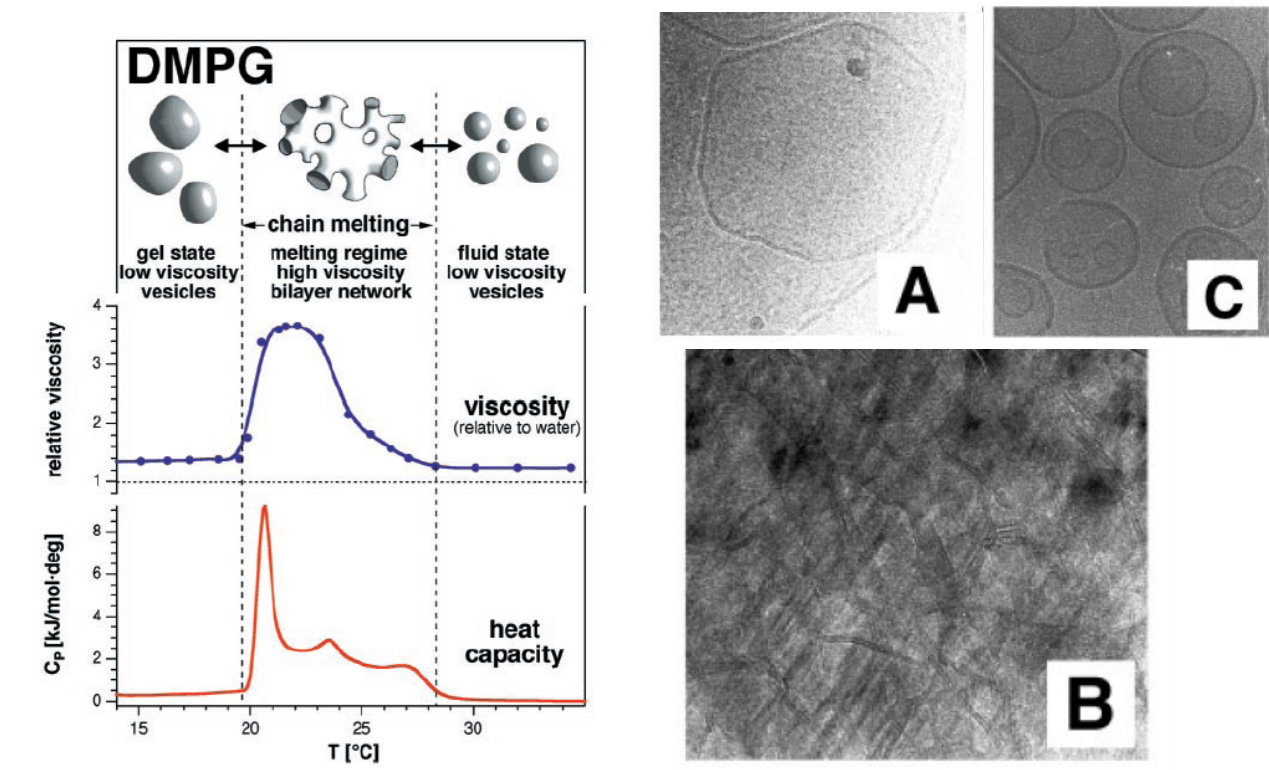


Figure 2.4: Schematic of Phase transition of DMPG (left). The bilayer network structure (sponge phase) is shown in the phase transition. Cryo-TEM micrographs of 15 mM DMPG (right). (A) Displaying large unilamellar vesicles (not spherical) at 15°C, (B) displays continuous membranes at 25°C and (C) displays unilamellar vesicles at 45°C. Adapted from [16]

Heat capacity profiles show that there occurs a continued acyl chain melting and a decreasing order throughout the entire phase transition. Despite the decrease in order during the phase transition it is more uncertain whether there occurs a decrease in the overall bilayer thickness. [17, 18] However

experiments using fluorescent anisotropy measurements [15] showed gradual decrease fluorescence anisotropy which is related to a decrease in acyl chain order. However it showed no sharp peak which indicates that the changes during the phase transition are indeed gradual. There occurs a great decrease of the chain packing at the beginning of the phase transition followed by a smooth decrease until the fluid phase is reached. Importantly, it has been confirmed [17, 18] that within the phase transition bilayer structures exist and the presence of multilamellar vesicles have been excluded. Additional experiments [17] have demonstrated that the bilayers most likely are packed into unilamellar vesicles. However highly disrupted membranes, or independent bilayer fragments have not been ruled out. In addition ESR spectra [15] indicate that two structurally different membrane domains exist within phase transition.

2.4.2 Theories

A theory by Schneider et al. in 1999 suggested that the phase transition consisted of a three-dimensional bilayer network like a sponge phase which could explain the increased viscosity and decreased transparency. [16] Experiments conducted [17] using labeled vesicles were passed through the phase transition several times by subsequent heating and cooling showed that the labels were retained within the initial vesicles. This showed that there cannot be any significant mixing of the vesicles in the phase transition. It also makes any fusion event within the phase transition unlikely. An explanation appeared for the increased viscosity and decreased light scattering in which the vesicles would aggregate in the gel and fluid phase and disaggregate in the phase transition. [19] Additional experiments [19] using fluorescence resonance energy transfer (FRET) on vesicles with donor and acceptor dyes. A lack of change in FRET efficiency means the donor and acceptor molecules did not interact, indicating that formation of aggregates in the gel and fluid phase seems unlikely. Other results [20] indicate that a net repulsive force exists in the phase transition.

To date there are two likely models [17] proposed for the phase transition. The first called the pore theory was proposed by Riske et al. (2004) and involved the formation of perforation within unilamellar vesicles in the phase transition. This theory could explain the increased conductivity as well as the increased transparency because light passes right through the holes. Experiments [17] in which the DMPG vesicles were cooled and reheated four consecutive times showed that the same vesicle was always observed in the fluid phase. This clearly demonstrates that the process is reversible and that the unilamellar vesicle structure is preserved during the phase transition. In addition, after keeping the vesicles in the phase transition for more than 15 minutes only small vesicles (size not specified) would appear. These measurements clearly support the pore theory. In these vesicles, highly curved positive surfaces occur which could help explain the increased viscosity and stabilizes the vesicle structure with these perforations. However whether the theory can explain the increase in overall viscosity is still uncertain.

The second model involves a change of the vesicle structure into elongated vesicles. In agreement with this theory is that elongated structures have been observed in the microscope. [16] In addition, if the vesicles have fragmented surfaces it appears likely that the vesicles will crumble during the phase transition but the process appears (almost) completely reversible.

Materials and Methods

3.1 Chemicals and samples

The DMPG lipids used were purchased from Avanti Polar Lipids (Alabaster, AL USA). For each DMPG sample the powder was slowly heated to room temperature to avoid water binding to the lipids the samples were then weighted off and stored in freezer at -18°C. Buffer solutions were initially made containing 10 mM NaCl buffer and 2 mM EDTA (Fluka) in millipore water. EDTA is used to prevent Ca^{2+} from the glass bottle into binding with the membranes. [21] Solutions containing 50 mM, 150 mM and 500 mM NaCl were made simply by adding additional NaCl to each buffer solution. All samples were created by weighting the required amount with an uncertainty of $\pm 0,0001$ g and dissolving into buffer solution.

The chosen buffers have a pK_a value close to the desired pH value to ensure that the pH is kept constant. NaOH and HCl was added to adjust the sample precisely to the correct pH within a margin of ± 0.01 pH using a pH meter (pH 538 purchased from WTW in Göttingen, Germany). The buffer solutions were stored in the fridge at 5°C.

pH	Buffer	pK_a pf buffer
4-5	Citric acid ($\text{C}_6\text{H}_8\text{O}_7 \cdot \text{H}_2\text{O}$) (AnalR)	4.77
6	MES ($\text{C}_6\text{H}_3(\text{NO}_2)_2\text{S} \cdot \text{H}_2\text{O}$) (Sigma)	6.15
7-8	HEPES ($\text{C}_8\text{H}_2(\text{N}_2\text{O}_4)_2\text{S}$) (Sigma)	7.48
9	TAPS ($\text{C}_7\text{H}_7(\text{NO}_6)_2\text{S}$) (Sigma)	8.43
10-11	Sodium bicarbonate (NaHCO_3) (Sigma)	10.32

For each experiment buffer solutions were added to the lipids, giving a 2 mM DMPG concentration. The sample was slowly heated and vortexed until the lipids were dissolved. For each experiment the sample was used only after the solution had been completely homogenous.

3.2 Vesicle preparation

Different techniques were required in order to create vesicle of different sizes for the DSC and rheology measurements as well as for the fluorescence microscopy.

3.2.2 Sonication

A Sonicator (Bandenlin SONOREX RK 31, Germany) was used to create vesicle of roughly 20 nm in size. The sample is simply inserted into a bath and ultrasound is applied for a few minutes to destroy larger vesicle structures.

3.2.1 Extrusion

Extrusion allows one to produce vesicles of certain sizes that ranged between 50 and 400 nm. The basic principle is to press the lipid solution through a filter purchased from Avestin Europe, Mannheim Germany), with pores of a specific size. This is repeated at least 30 times at 45°C. The extruded vesicles will have roughly the same size as the pore sizes. The machine used for the extrusion was homemade in our lab as seen in picture 3.1.

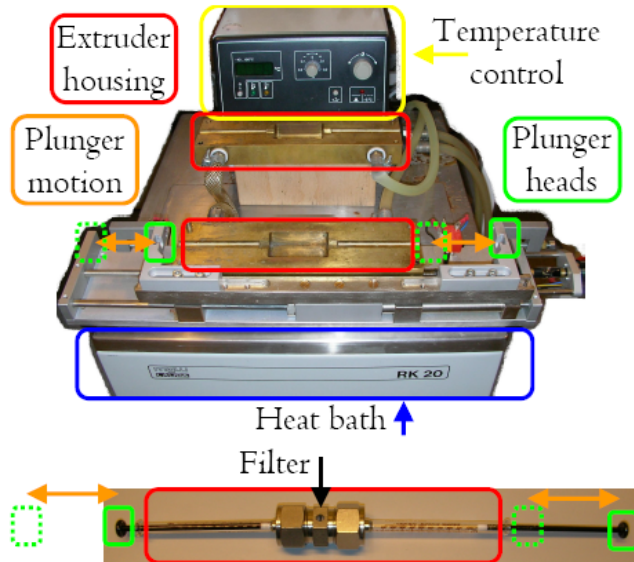


Figure 3.1: layout of extrusion instruments. Two syringes are attached on each side of a meal block containing a filter. One syringe contains the lipid solution (960 µl). The membrane along with the syringes, are placed inside the extruder housing which is connected to a heat bath. Plunger heads are placed in holders which are electronically controlled, moving with a frequency of 1 cycle per minute. [6]

3.2.3 Evaporation

For the fluorescence microscopy measurement it was necessary to create giant vesicles using an evaporation procedure. 10 mg DMPG was dissolved in 960 µl chloroform and methanol solutions ranging between 100-200 µl. Different DMPG concentrations were used ranging between 2-6 mM. 2µl of a solution containing methanol/dichloromethane at a ratio of 1:2 and the DiI (1,1'-Diocadecyl-3,3,3',3'-tetramethylindocarbocyanine perchlorate) dye with a concentration $5.9 \cdot 10^{-4}$ mM was added, (giving a 1:10.000 molar ratio to DMPG). The sample was evaporated using an air tube blowing nitrogen until it was dry. The sample was placed inside a vacuum chamber for 2 hours to remove the organic solvent and 1 ml buffer solution was added. [22] Note: sample was kept dark in order to protect the dye.

3.3 Viscosity

Viscosity is a measure of a fluid's thickness or resistance to being deformed under stress. Higher thickness of the fluid means higher viscosity.

The viscosity was measured using a rotation rheometer from Contraves (Switzerland) called Low Shear 30 Sinus. The rotational rheometer functions by applying a force on the sample in order to determine its viscosity. A small metal cup is filled with the sample and rotated with a constant velocity. A pendulum is placed into the center of the solution so that its entire weight is covered by the sample. The liquid causes the pendulum to rotate and the rotational force (torque) is measured. The torque is proportional to the rotation speed of the pendulum, and thus to the viscosity of the fluid. Importantly, increasing the scanning rate also increases the viscosity range of the sample. [3] It is essential to have as low scanning rate as possible in order to allow the system to reach equilibrium properly during each measurement. Each experimental run was performed with a scan rate of 7°C/hour in the measurement range of 5 – 50°C.

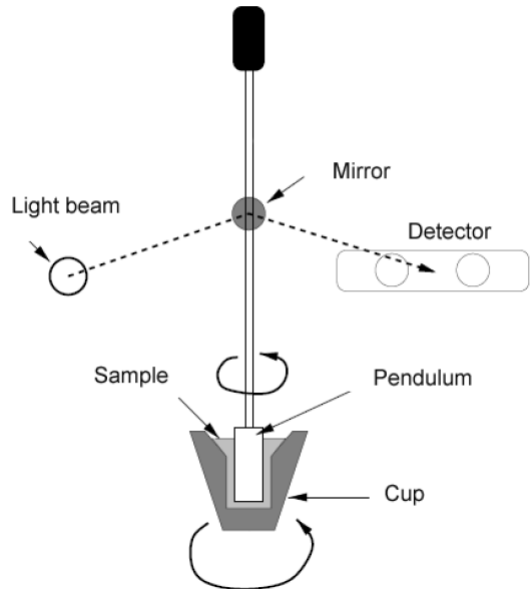


Figure 3.2: Simplified drawing of rheometer.
Taken from thesis of Peter Grabitz 2001.

The pendulum was calibrated to be positioned in the center of the solution in order to minimize perturbations in the viscosity as a result of variations of pendulum-cup distance. The apparatus was isolated from surroundings in order to control the temperature variation and a water tank (regulator) was used to regulate the temperature in the experiment range. The regulator operated in conjunction with a thermometer positioned underneath the metal cup to constantly readjust the temperature. A water reservoir inside the isolation prevented the sample from drying out during each long run.

3.4 Differential Scanning Calorimetry

3.4.1 Principles

Differential scanning calorimetry (DSC) is a technique for the study of both thermally or conformationally induced transitions whether they are exothermic or endothermic in nature. [23] A DSC has two cells that are isolated adiabatically. One cell contains the sample while the other cell contains a reference solution. During the scan the temperature is regulated at a constant scan rate so that the difference in temperature between the two cells is zero. The difference in power/heat needed to adjust the temperature between the two cells is a measure of the different processes taking place in the two cells. [2]

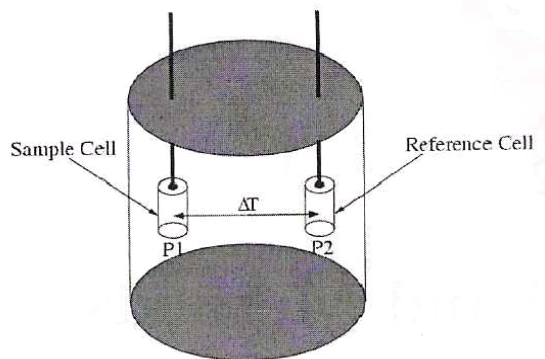


Figure 3.3: Schematic drawing of the cell of the Differential scanning calorimeter DSC. [2]

Through this relation we derive that DSC measures the excess heat capacity (C_p) of the sample of interest is basically a derivative of the enthalpy change (at constant pressure):

$$C_p = \left(\frac{dH}{dT}\right)_p \quad (3.1)$$

The lipids have a heat capacity different from zero outside the phase transition. This leads to an enthalpic contribution to the heat capacity profile in addition to the phase transition. Removing this contribution is called subtracting the baseline which will be discussed in section 3.6.

3.4.2 Experiment

Heat capacity measurements were obtained using a VP differential scanning calorimetry from MicroCal (Northhampton, MA, USA). Each cell contained 0.5152 ml solution. The reference cell contained millipore water while the other contained the DMPG lipid sample. Before every scan a constant pressure of approximately 50 psi was obtained. VP-Viewer program was used to run the experiments and control the parameters. Three scans were run in total at a scan rate of 5°C/hour, two upwards and one downwards. The starting temperature was set to 5°C and the final temperature to 40°C. The time interval for each filtering period was set to 5 seconds and a high feedback was chosen. This ensures that the calorimeter reacts fast to changes in the system.

3.5 Fluorescence microscopy

The sample was put into a small plastic chamber. The chamber was then inserted into a metal plate covering the sample. The metal plate was connected to a water tank in order to regulate the temperature of the sample. The plate was put on top of the fluorescence microscope (Olympus IX 71 purchased from Olympus America Inc. in USA) and measurements were taken using a program called maxim. The dyes bleach rapidly under a fluorescent light so it was essential to observe events for very brief periods of time at each given location and to keep a low intensity. Pictures were taken using a charge-coupled device (CCD) camera that needs to be heated and cooled slowly in order to avoid moisture.

Data analysis

4.1 Rheology

The rheometer produces a number through the speed of its rotation that is proportional to the fluids viscosity. This number can be used to calculate the viscosity relative to other solutions. The samples containing DMPG were compared relative to the buffer solution with 10 mM NaCl at pH 7. To find the relative viscosity of the different samples each data point of the sample measurement was divided with the buffers measured viscosity at the same temperature.

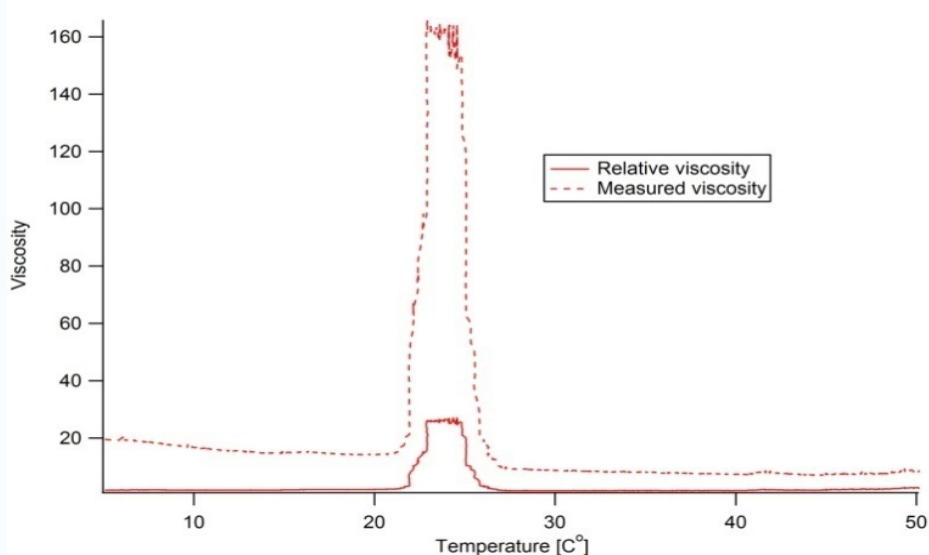


Figure 3.4: Measured viscosity versus the relative viscosity where all the points have been divided with the buffer solution. Shown for pH 11 at 10 mM NaCl.

LabVIEW was used to measure the viscosity of the samples at a constant scan rate of 7°C/hour. As determined from previous experiments [] this sample rate gives necessary and sufficient time to allow the system to equilibrate between each measurement including within the interval where the viscosity is high.

4.2 Differential scanning calorimetry

The IgorPro program was used with a macro to remove the baseline from the heat capacity curves. This ensures that the resulting signal only corresponds to the lipids. The transition temperature corresponds to the transition peak at the maximal peak height, and the transition enthalpy is equal to the integrated area under the peak after removal of the baseline. The procedure is to remove the transition peaks from the heat capacity curve and then fitting the resulting curve with a polynomial function of degrees between 3 and 5. The fit was then subtracted from heat capacity curve giving a heat capacity change corresponding exclusively to the phase transition.

Results

5.1 pH and NaCl dependence

5.1.1 DSC profiles

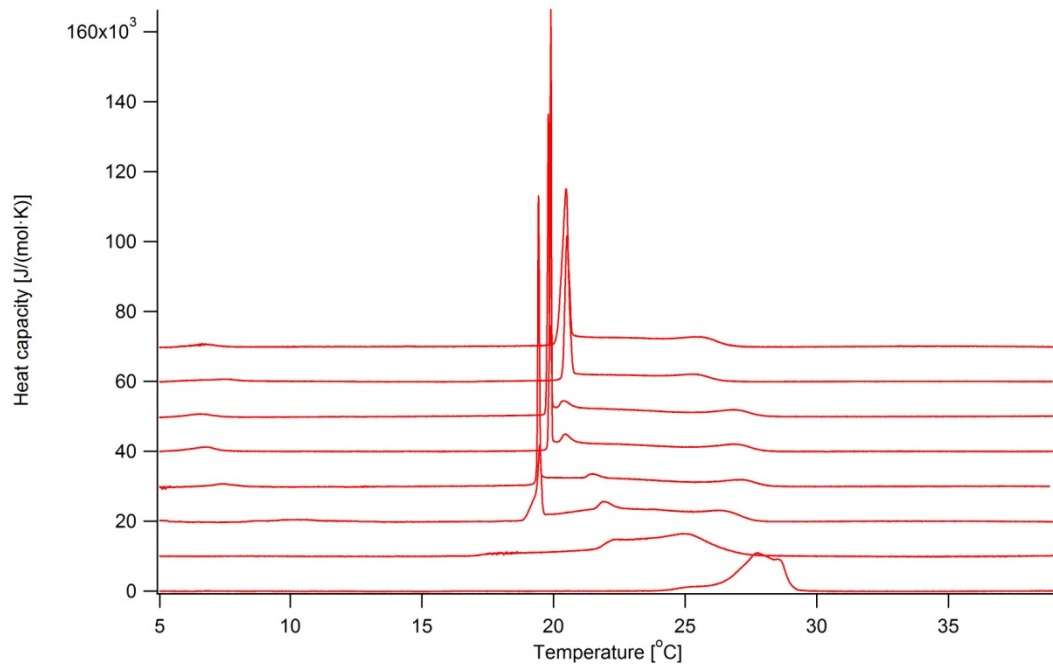


Figure 5.1: Heat capacity profiles of DMPG at 10 mM NaCl with a pH range of 4 to 11. Lowest profile represents pH 4 and highest shows pH 11.

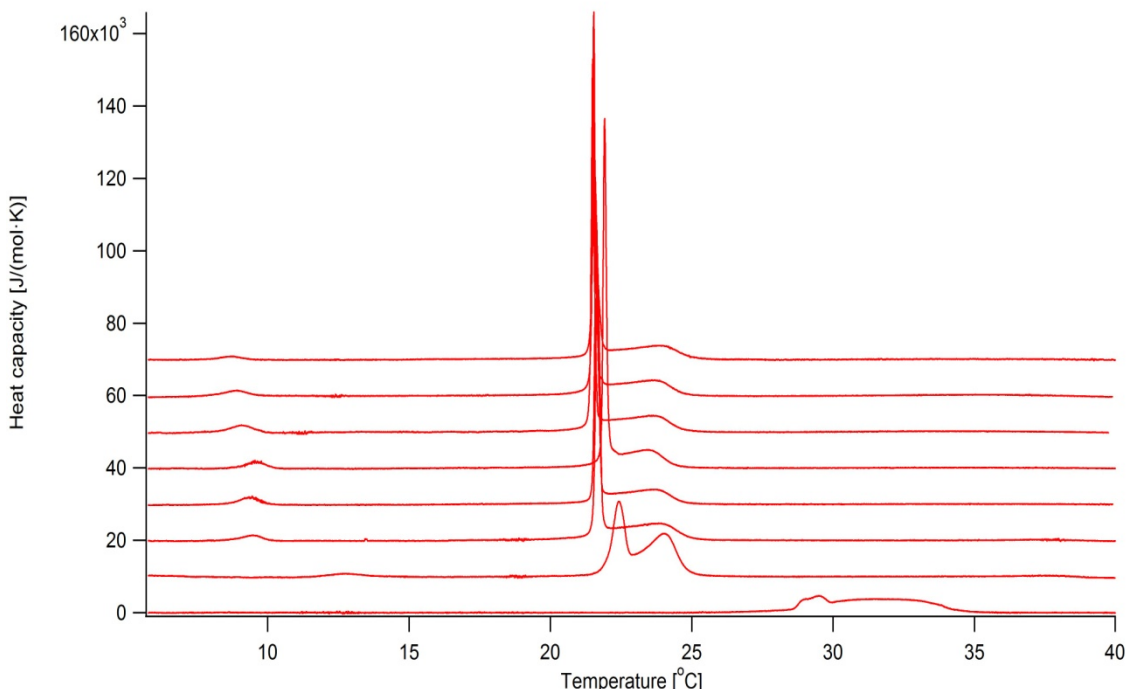


Figure 5.2: Heat capacity profiles of DMPG at 50 mM NaCl with a pH range of 4 to 11. Lowest profile represents pH 4 and highest shows pH 11.

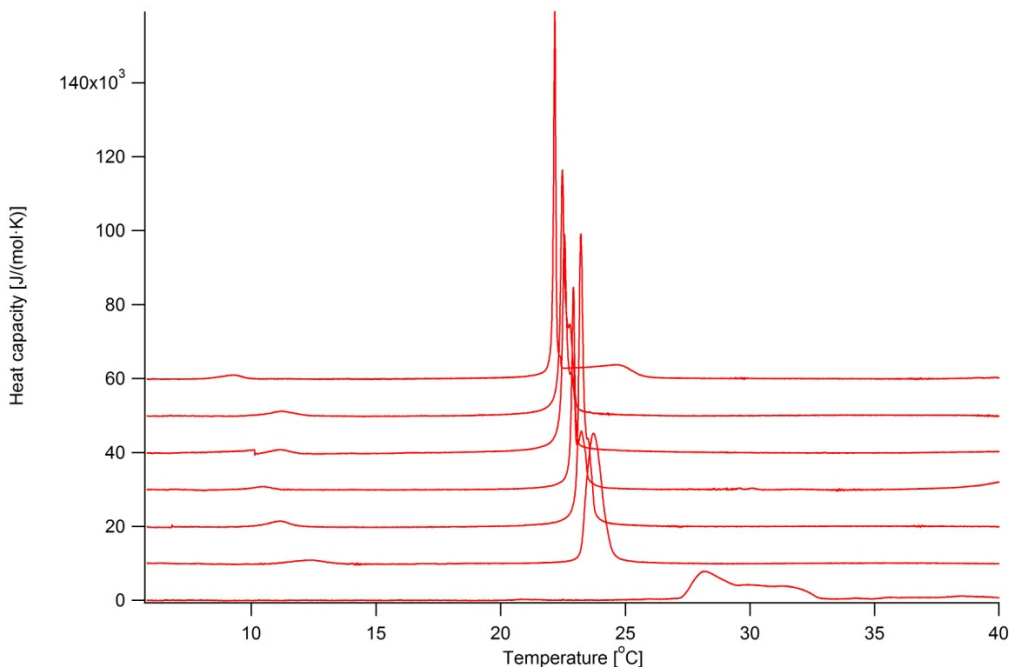


Figure 5.3: Heat capacity profiles of DMPG at 150 mM NaCl with a pH range of 4 to 11. Lowest profile represents pH 4 and highest shows pH 11.

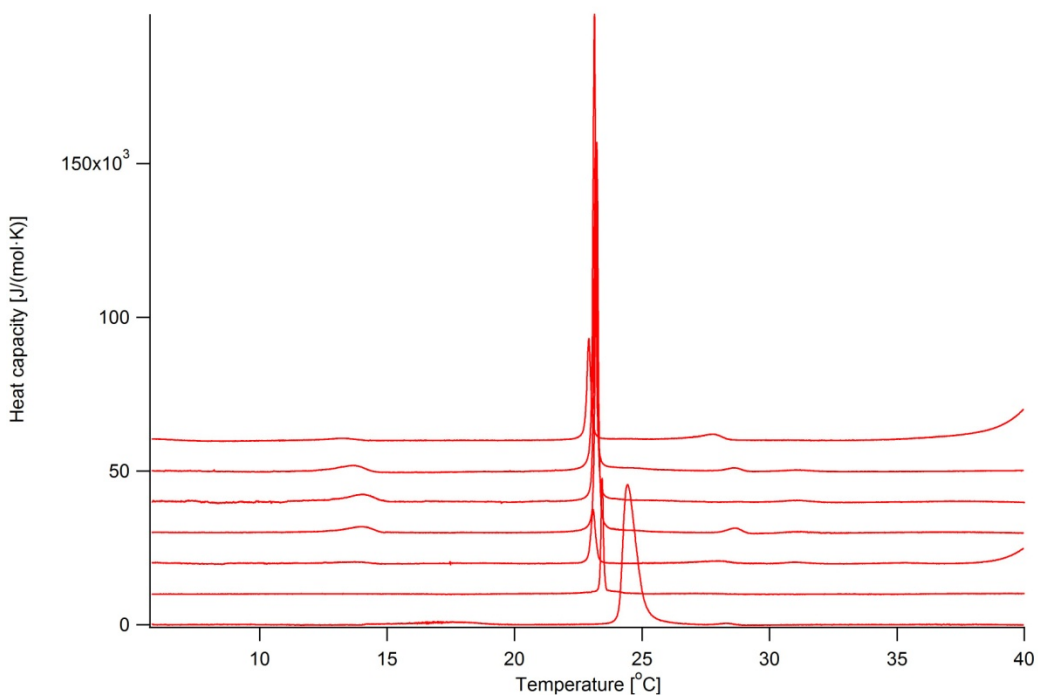


Figure 5.4: Heat capacity profiles of DMPG at 500 mM NaCl with a pH range of 4 to 11. Lowest profile represents pH 4 and highest shows pH 11.

The heat capacity profiles after subtraction of baseline are shown above with different NaCl concentrations and a pH range of 4-11. Only one scan was chosen from each experiment and the resulting profile for each pH value was compared with the other pH values as shown in figure 8-11.

For pH 6 and above the 3 different scan profiles similar behavior for all NaCl concentrations (not shown). The difference between them is that they exhibit a general shift in the phase transition at different scans. At 10 mM to 50 mM NaCl the phase transition lowered at later scans while at 500 mM NaCl the phase transition increased at later scans. The different scans below pH 6 (not shown) showed lack of reversibility and reproducibility.

The profiles can be categorized as follows:

10 mM NaCl:

- for pH 6-9 the heat capacity profile shows the characteristic broad transition between 18-28 °C with three peaks while the first peak being very sharp, then a small narrow peak in the middle of the melting regime and ending in a small broad peak.
- For pH 4-5 the profile changes into fewer peaks and the transition regime narrows.

50-500 mM NaCl:

- Increasing NaCl concentrations narrows the phase transition until it reaches a single narrow peak for all pH values ≥ 5 . The smaller peaks also disappear.
- Increasing NaCl concentrations increases the phase transition temperature for all pH values ≥ 6 .

5.1.2 Viscosity profiles

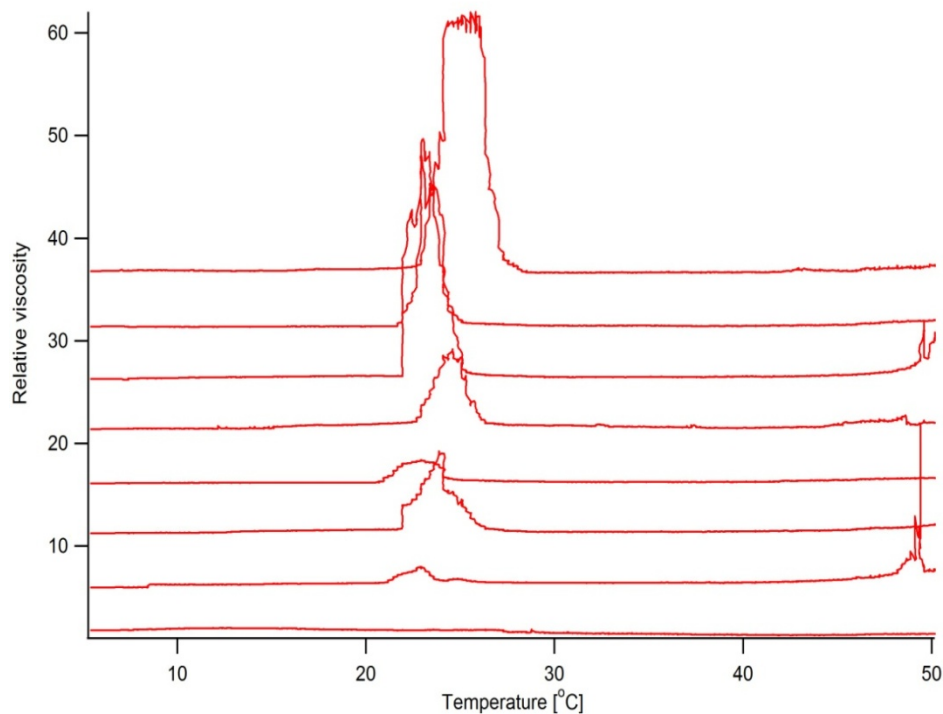


Figure 5.7: Relative viscosity of DMPG at 10 mM NaCl with a pH range of 4 to 11. Lowest profile represents pH 4 while highest shows pH 11.

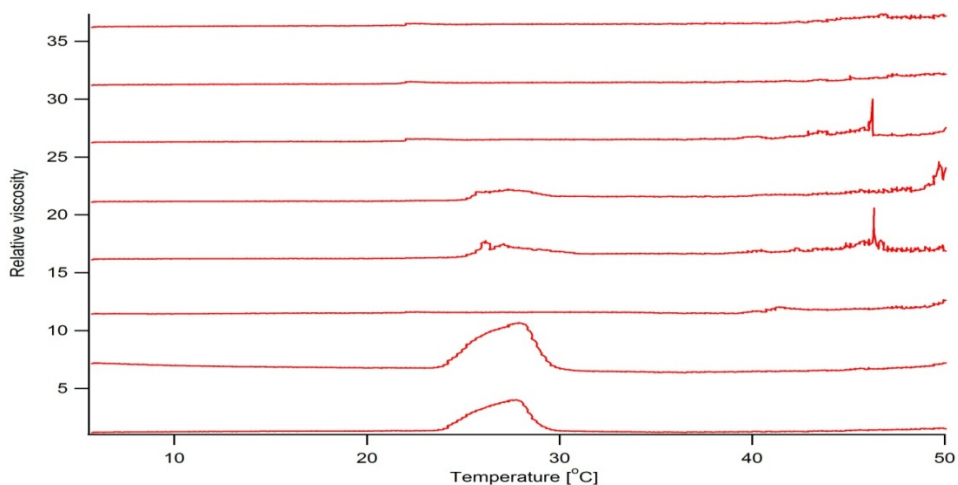


Figure 5.8: Relative viscosity of DMPG at 50 mM NaCl with a pH range of 4 to 11. Lowest profile represents pH 4 while highest shows pH 11.

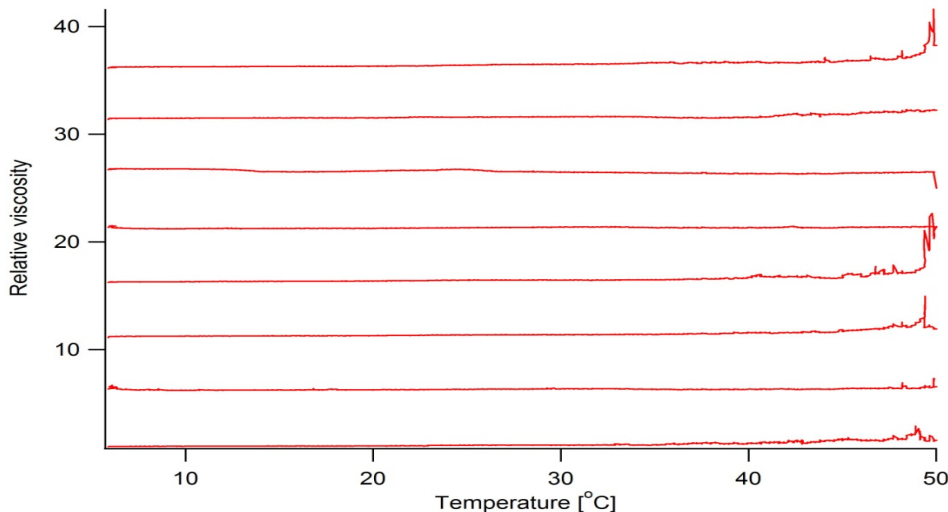


Figure 5.9: Relative viscosity of DMPG at 150 mM NaCl with a pH range of 4 to 11. Lowest profile represents pH 4 while highest shows pH 11.

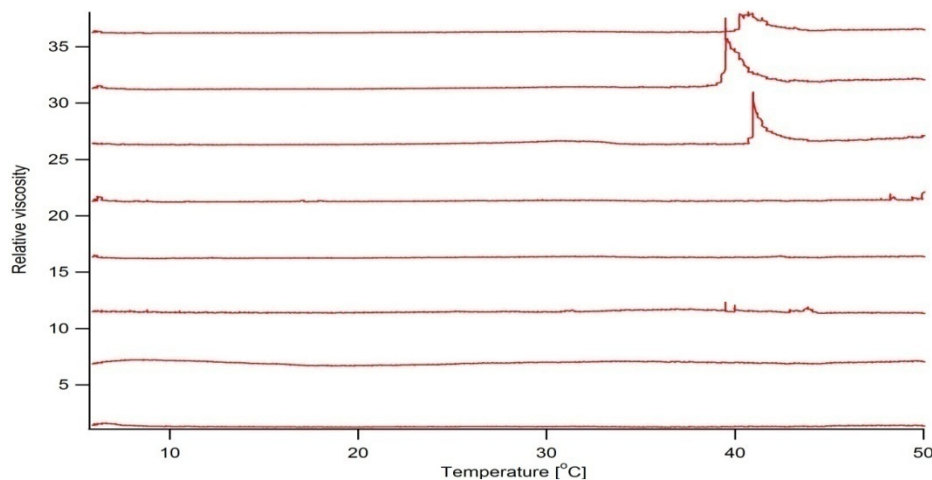


Figure 5.10: Relative viscosity of DMPG at 500 mM NaCl with a pH range of 4 to 11. Lowest profile represents pH 4 while highest shows pH 11.

The relative viscosity of the DMPG samples with different NaCl concentrations and a pH range of 4-11 are shown above. The viscosity profiles were run from 5°C to 50°C at a rate of 7°C/hour. The profiles can be categorized as follows:

10 mM NaCl:

- The relative viscosity appears to generally increase with increasing pH except for pH 7
- The high viscosity region is similarly wide for all pH ≥ 6 although a widening of the region appear to occur with increasing pH.

50 mM NaCl:

- The viscosity decreases with increasing pH.

150-500 mM NaCl:

- Increasing NaCl concentration decreases or removes the high viscosity region.

5.2 Vesicle sizes

5.2.1 DSC profiles

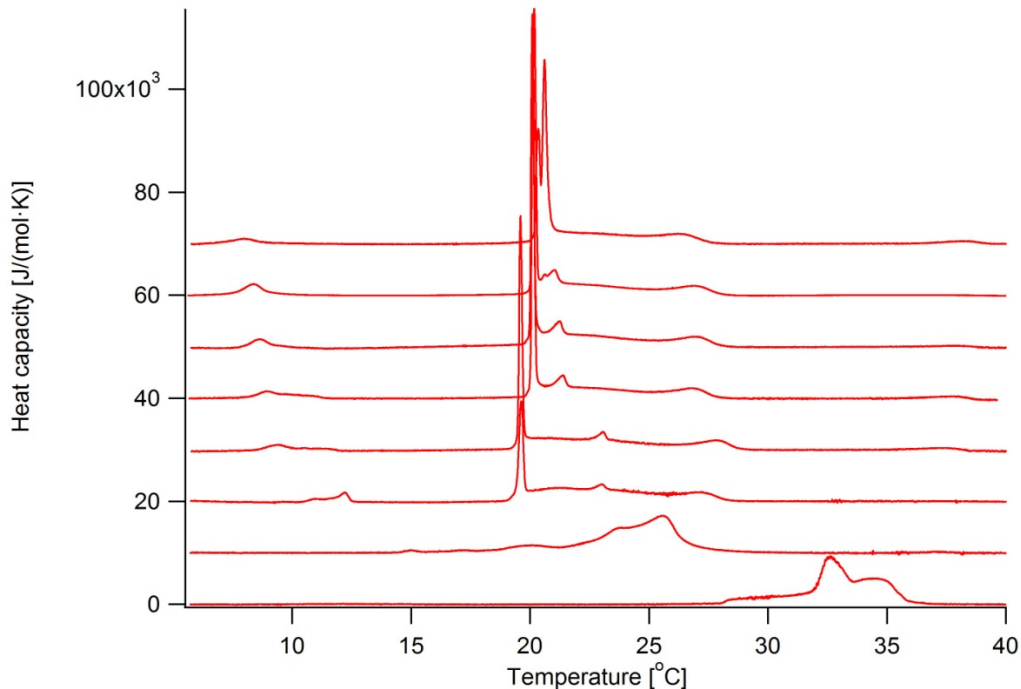


Figure 5.11: Heat capacity profiles of DMPG of a 20 nm vesicle sizes within a pH range of 4 to 11. Lowest profile represents pH 4 and highest shows pH 11.

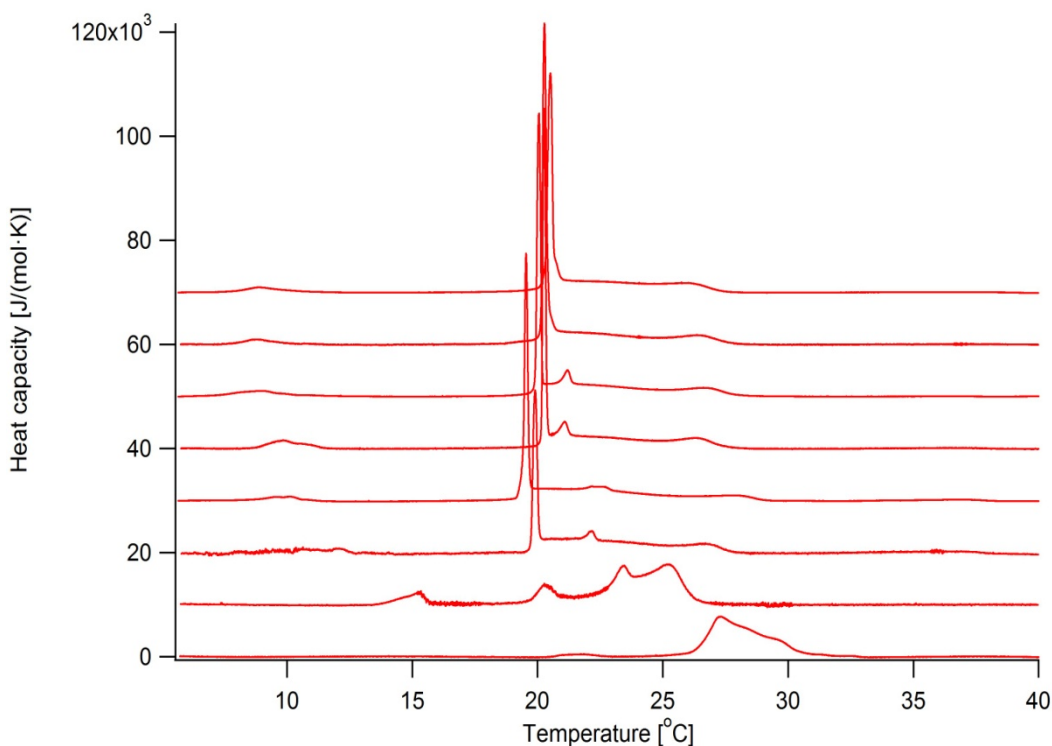


Figure 5.12: Heat capacity profiles of DMPG of a 100 nm vesicle sizes within a pH range of 4 to 11. Lowest profile represents pH 4 and highest shows pH 11.

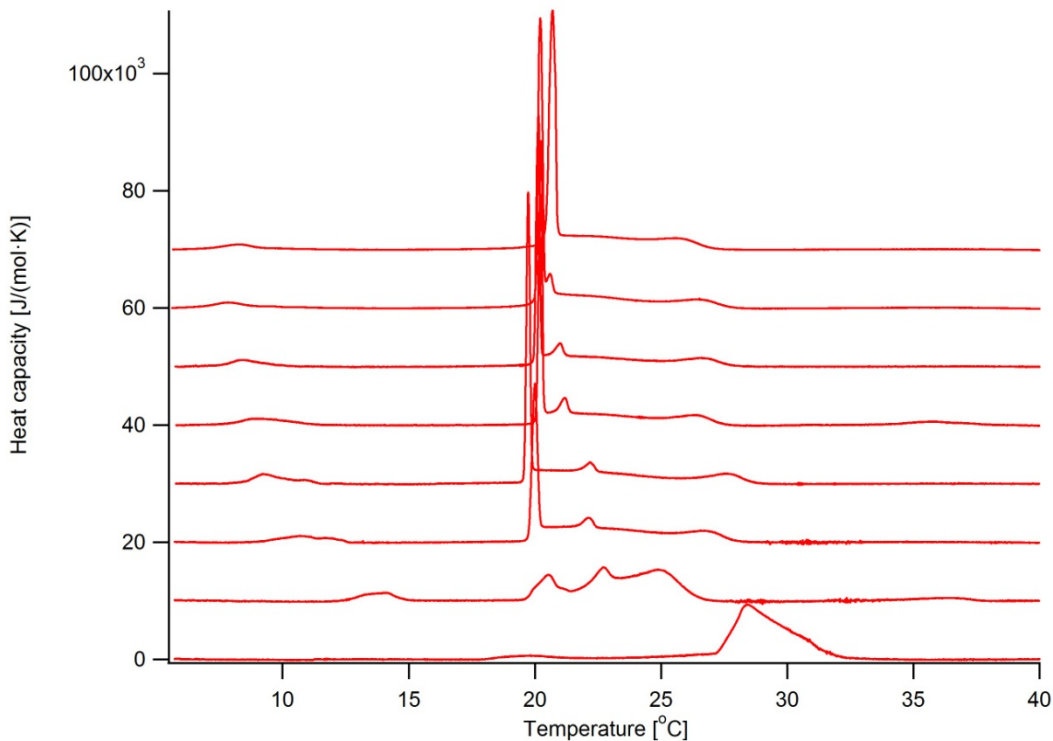


Figure 5.13: Heat capacity profiles of DMPG of a 400 nm vesicle sizes within a pH range of 4 to 11. Lowest profile represents pH 4 and highest shows pH 11.

Heat capacity profiles of the DMPG samples were obtained for different vesicle sizes within a pH range of 4-11. By comparing the different graphs it is seen that the melting behavior is very similar for different vesicle sizes. However a few observations can be made:

- The broadness of the peak appear to be the same for the different vesicle sizes.
- The vesicles of larger size appear to have a higher main peak than that of the smaller vesicles.
- For pH ≤ 5 the phase transition is lowered for the larger vesicles.
- The second peak appears a little more pronounced for the larger vesicles.

5.2.2 Viscosity profiles

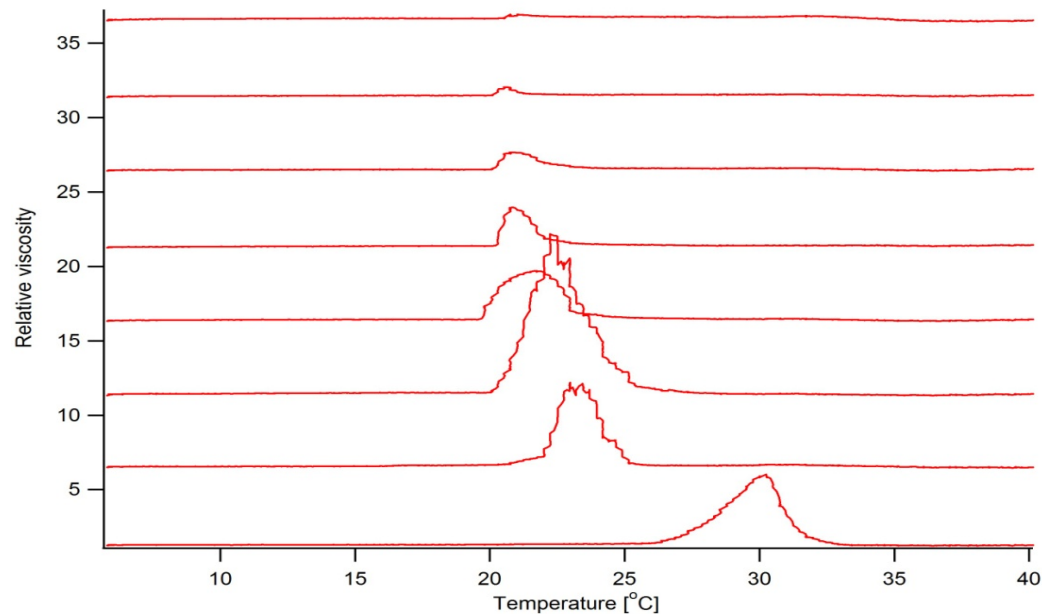


Figure 5.14: Relative viscosity of DMPG vesicles 20nm in size with a pH range of 4 to 11. Lowest profile represents pH 4 while highest shows pH 11.

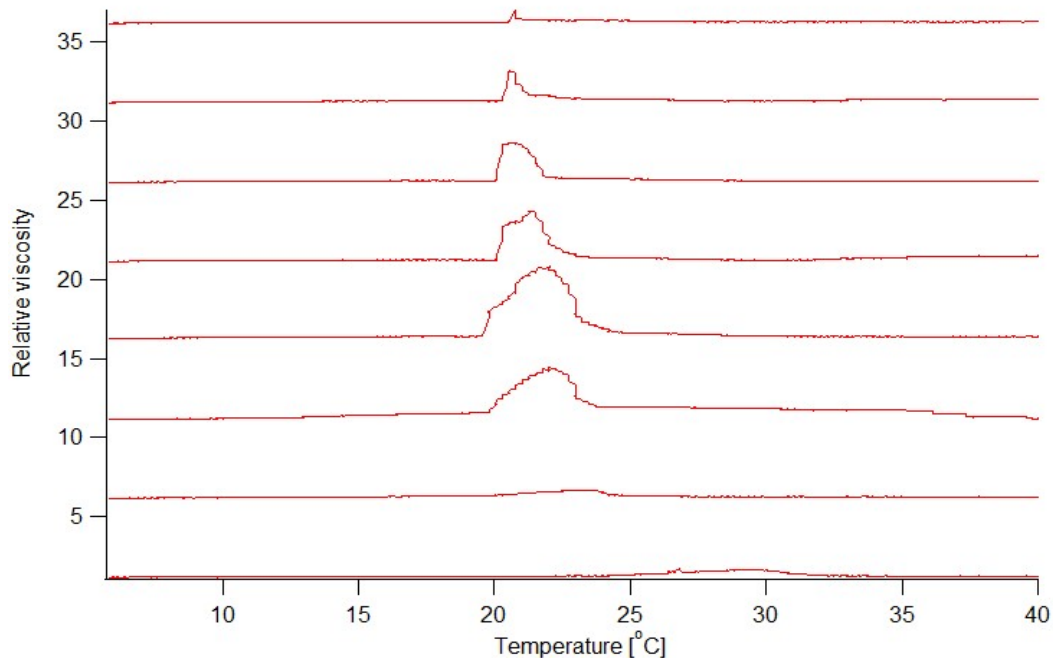


Figure 5.15: Relative viscosity of DMPG vesicles 100nm in size with a pH range of 4 to 11. Lowest profile represents pH 4 while highest shows pH 11.

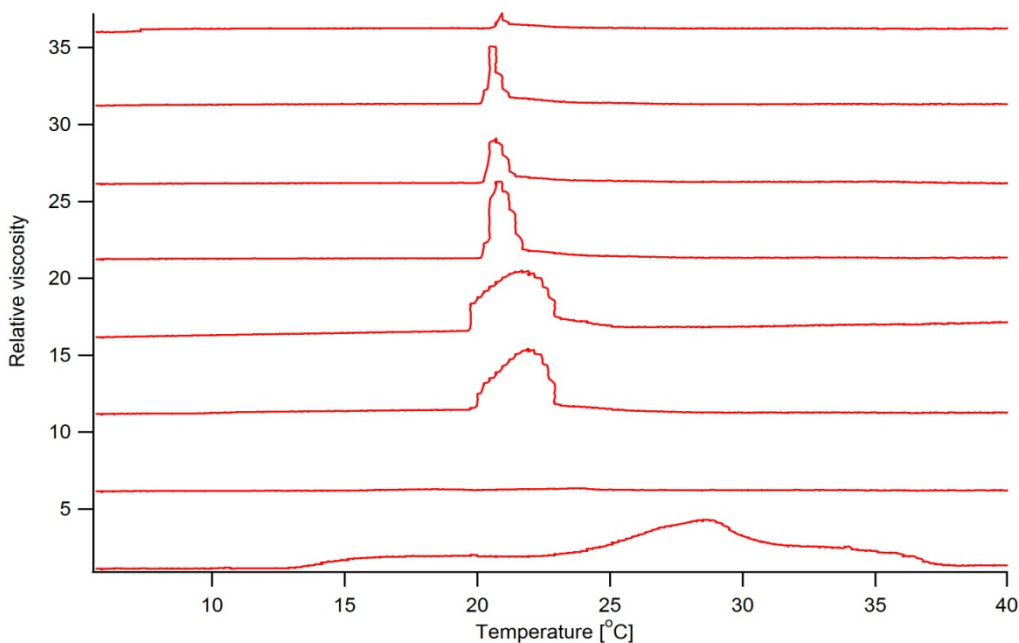


Figure 5.16: Relative viscosity of DMPG vesicles 400nm in size with a pH range of 4 to 11. Lowest profile represents pH 4 while highest shows pH 11.

The relative viscosity of the DMPG samples with different vesicle sizes within a pH range of 4-11 is shown above. The viscosity change in the phase behavior is drastically different by comparing the different vesicle sizes. The following observations were made:

- For all vesicle sizes the broadness of the high viscosity region decreases with increasing pH.
- The maximal value of the viscosity in the phase transition increases for pH 5-6 and decreases for pH ≥ 7 with increasing pH.
- The viscosity appears generally similar in height and broadness for the different vesicle sizes at pH ≥ 7 .
- For pH 4 the broadness of the phase transition increases with increasing vesicle sizes.
- The shapes of the high viscosity region are similar for the different vesicle sizes and are very different than for the melting behavior of unprepared DMPG solutions.

5.3 Area expansion

The area compressibilities for different vesicle sizes were calculated using equation 2.4 and the constants for DMPC for the gel and fluid phases. The graphs were also compared with DMPG in a 10 mM NaCl solution.

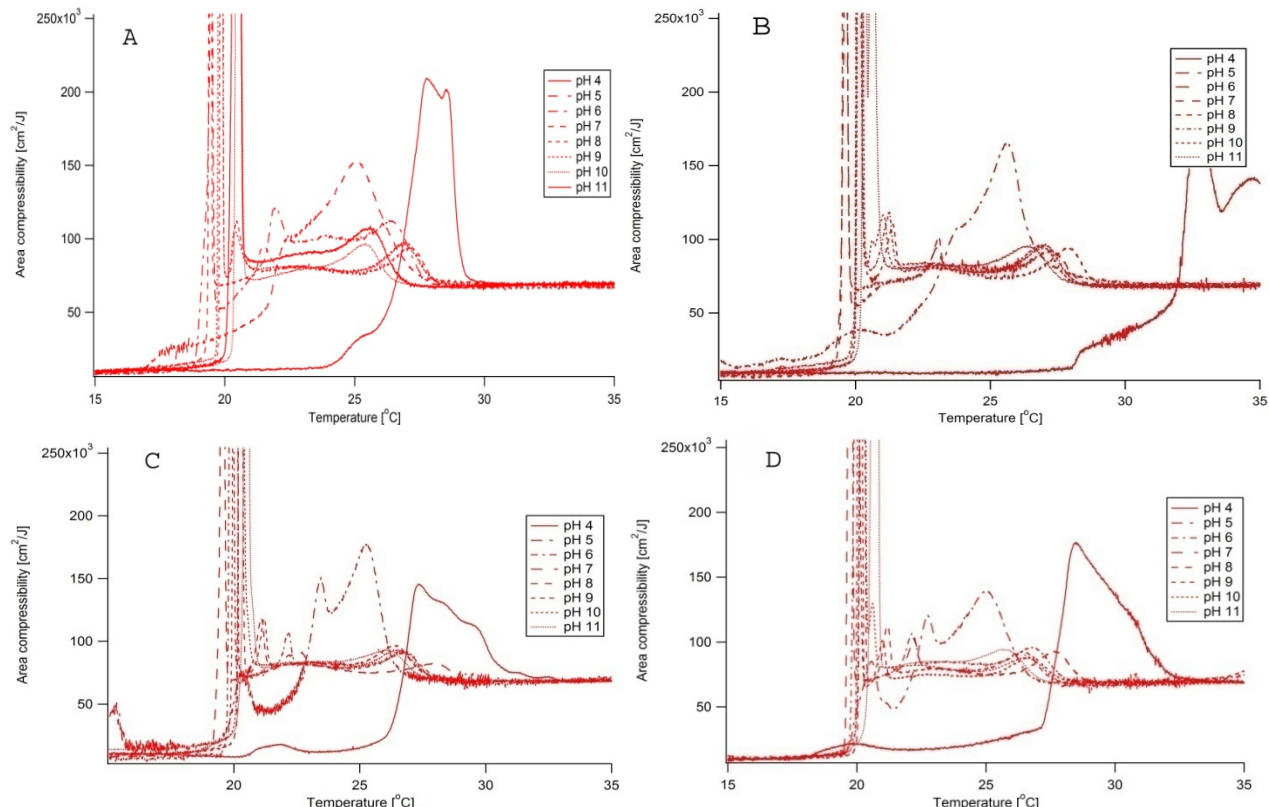


Figure 5.18: graphs of the area compressibility for different vesicle sizes within a pH range of 4-11. (A) 10 mM NaCl, (B) 20 nm vesicles. (C) 100 nm vesicles and (D) 400 nm vesicles.

The area compressibilities have the general feature of having the area compressibility of the gel phase below the phase transition, then a huge change in the phase transition occurred, followed by a stabilization of the area compressibility to that of the fluid phase above the phase transition. This behavior is exactly what one would expect for the change in the area compressibility. Some observations were possible by comparing the graphs:

- At 10 mM NaCl concentration the area compressibility for the different pH ≥ 6 appears highly variable between the second and third peak. This variation decreases when using vesicles of the same size.
- At different vesicle sizes the changes in the area compressibility occur at approximately the same temperature.
- The area compressibility is under nearly all circumstances higher in the phase transition than in the fluid phase.
- A main feature of the different pH is that at higher pH the area compressibility has additional peaks right after the main peak and the peak closes in on the main peak at increasing pH.

5.4 Bending modulus

Using equation 2.3 the bending modulus for different vesicle sizes were obtained within a pH range of 4-11. Each curve was smoothed by averaging the values for every 10 values in order to reduce the noise. The graphs were also compared with DMPG in a 10 mM NaCl solution.

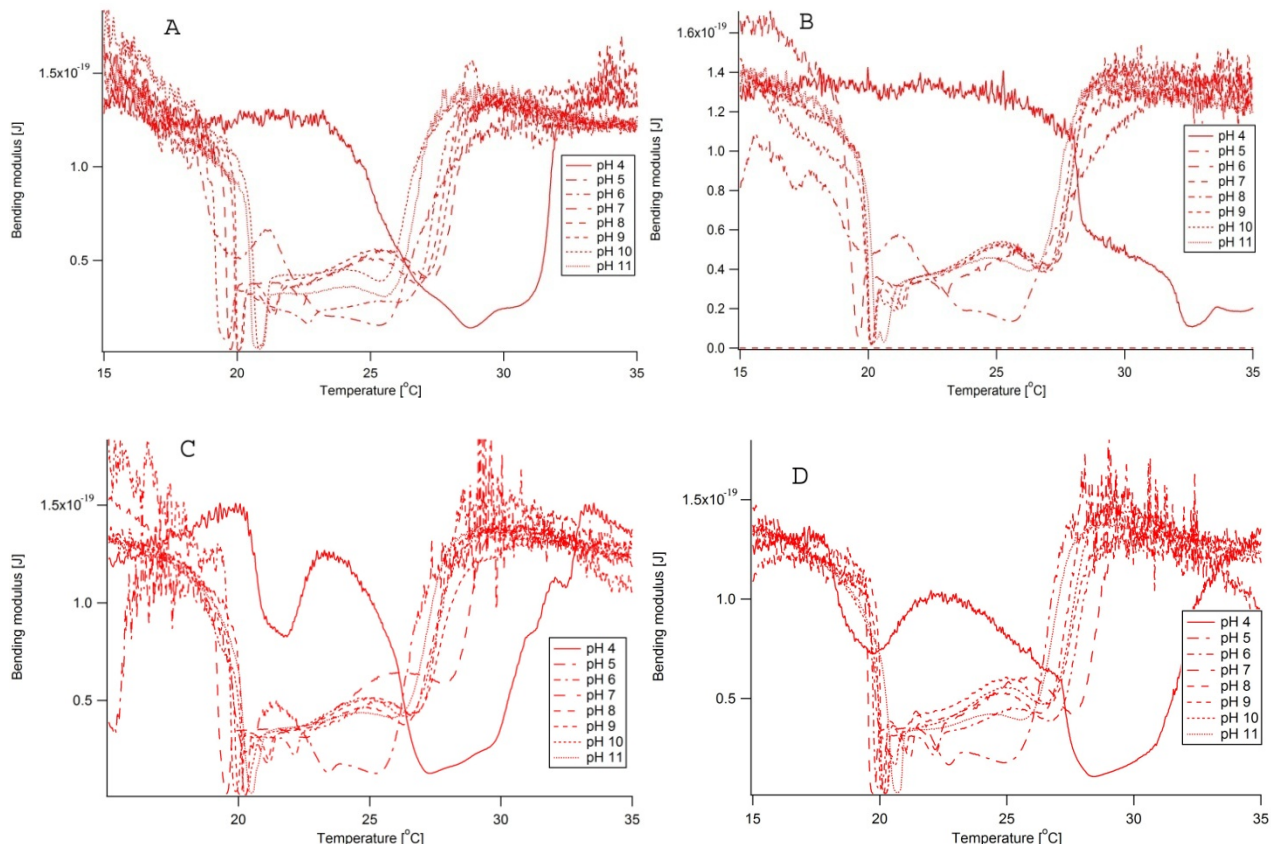


Figure 5.19: graphs of the bending modulus for different vesicle sizes within a pH range of 4-11. (A) 10 mM NaCl, (B) 20 nm vesicles. (C) 100 nm vesicles and (D) 400 nm vesicles.

Some interesting observations were made by comparing the graphs:

- A general feature of the bending modulus is that it is lower in the phase transition by an order of magnitude than either the gel or the fluid phase.
- At small vesicle sizes (20 nm – 100 nm) the variance in the bending modulus for the different pH is lower than the naturally dispersed solution (A) and the larger vesicles (D). The variance increases with increasing vesicle sizes.
- A main feature of the different pH is that at higher pH the bending modulus has additional peaks right after the main peak and the peak closes in on the main peak at increasing pH.
- At pH below 7 the bending modulus first becomes low at higher temperature.

5.5 Fluorescence Microscopy

Fluorescence images were obtained using DMPG solutions at pH 7. The best images were at 100 µl methanol and 6 mM DMPG. During some of the experiments it was not possible to regulate the temperature due to the regulator was damaged. However for some experiments the temperature could be regulated and observations could be made:

- 40°C, **Above phase transition**: small vesicles were observed in different shapes, mostly spherical.
- Approximately 20°C, **lower end of phase transition** (this is uncertain due to damaged regulator): an enormous variety of different structures were observed. In the optical microscope a giant vesicle was observed having deformations looking like rivers (figure 5.20) and small vesicle formed like a string of pearls on tubular structures (figure 5.21).

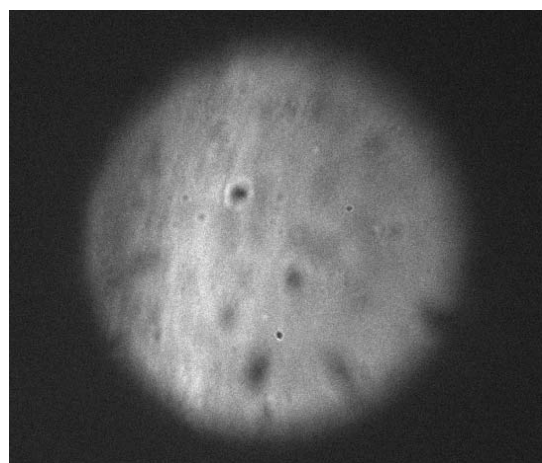


Figure 5.20: Giant vesicle observed with rivers in fluorescence microscope at approximately 20°C.

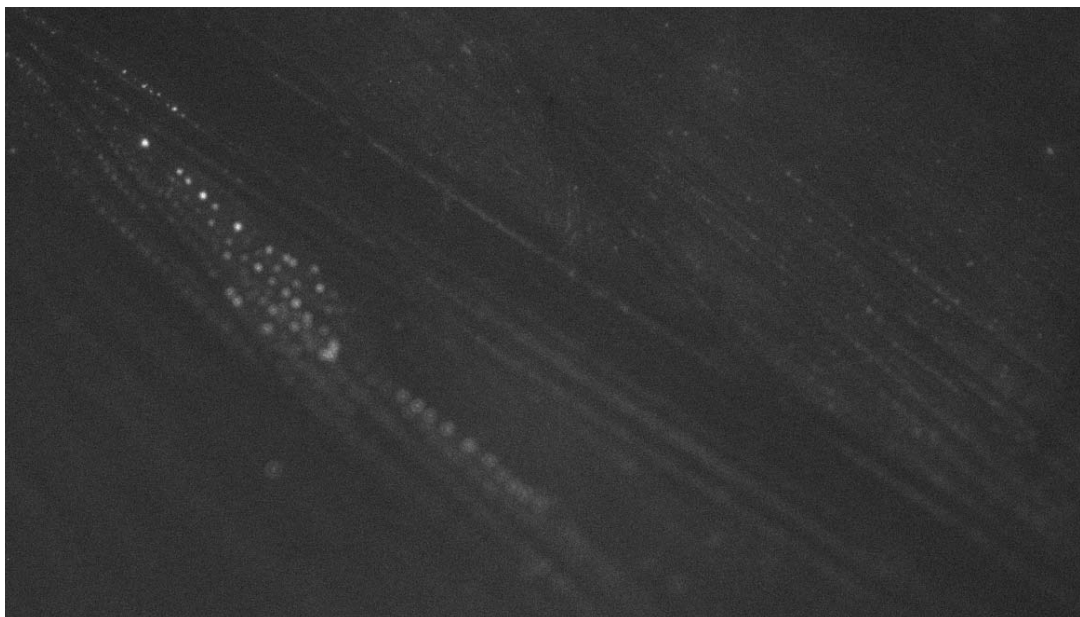


Figure 5.21: Small vesicles arranged like a string of pearls on tubular structures at approximately 20°C.

Discussion

6.1 pH and ionic dependence

6.1.1 DSC profiles

In figure 5.1 one can observe two different heat capacity curves: for pH 4-5 there appears to be only one peak and at pH ≥ 6 a broad phase transition with three peaks. For pH 6-9 the width of the phase transition is close to constant and then begins to narrow at pH 10-11. The beginning temperature for the main peak in the phase transition lies in a very narrow temperature region for pH ≥ 6 . Also at pH above 6 the temperature region of the phase transition appears to remain constant. This indicates that in this pH range the phosphate groups are close to fully deprotonated. The narrowing of the phase transition at increasing pH might be due to increased charge repulsion. The lowering of pH below 6 induces the disappearing of the peculiar phase behavior and the temperature of the phase transition increases as predicted due to the neutralization of the charged headgroups, resulting in a stabilization of the gel phase.

Increasing the ionic strength narrows the phase transition regime until it reaches a single peak at > 100 mM NaCl for pH ≥ 6 . In accordance with previous experiments, this shows that the peculiar phase transition only occurs at low salt concentration.

As previously explained the enthalpy change (figure A.1) during the phase transition appears approximately the same for the different NaCl concentrations (discounting degraded samples). This suggests that the chain melting is spread over a large temperature range.

These results show that the phase behavior is highly dependent on the ionic strength and pH of the sample.

6.1.2 Viscosity curves

In figure 5.7 an average increase in the relative viscosity with increasing pH appears to be the trend except for pH 7. In other words the deprotonation of the phosphate groups and thus the degree of dissociation appear to play a major role for the increased viscosity. Unlike the DSC profile which suggests that deprotonation is complete at pH 6 the viscosity continues to increase. This suggests that although the membrane is fully deprotonated at pH 6 the charge repulsion continues to rise, giving a higher degree of dissociation. At pH 9-11 there appear to be a certain limit in the maximal amount of viscosity. This could be due to the possibility that the vesicles are dependent on other properties other than surface charge such as bending of the membranes.

At 50 mM NaCl (figure 5.8) the high viscosity region lies at pH 4-5 and the viscosity decreases with increasing pH. The decrease in viscosity suggests that at high ionic strength the phase transition is already disrupted and the increasing dissociation disrupts it even more.

The fact that there still occurs high viscosity at low pH further strengthens that the peculiar phase behavior is dependent on pH. These results taken together could suggest that different morphological changes might occur at the phase transition below pH 6.

6.1.3 Heat capacity and viscosity curves compared

Heat capacity profiles and the relative viscosity curves were plotted for the same pH in the same figures (figure 6.1-6.2). The curves are for 10 mM NaCl concentrations. The viscosity curves were shifted to the right in order to give better correspondence with the heat capacity profile. A very likely reason is that the thermometer in the viscometer measures temperatures that are a little higher than that of the DSC. In other words different thermometers measure the same relative change but not necessarily the same absolute value.

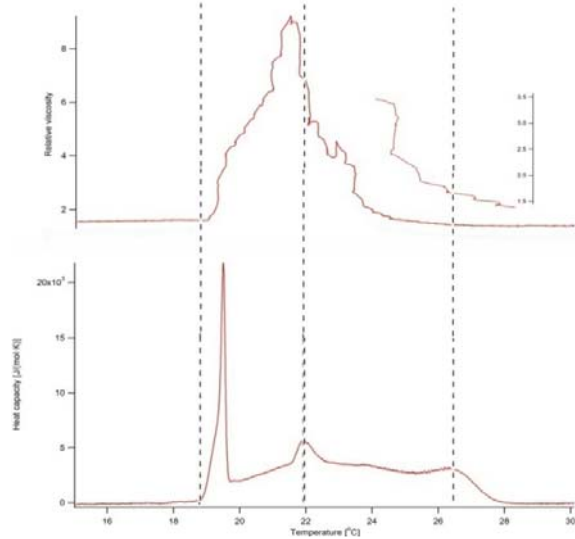


Figure 6.1: Viscosity and heat capacity curves for pH 6. Left viscosity axis is for the full viscosity curve. The right axis and the other curve shows a zoom of a part of the curve.

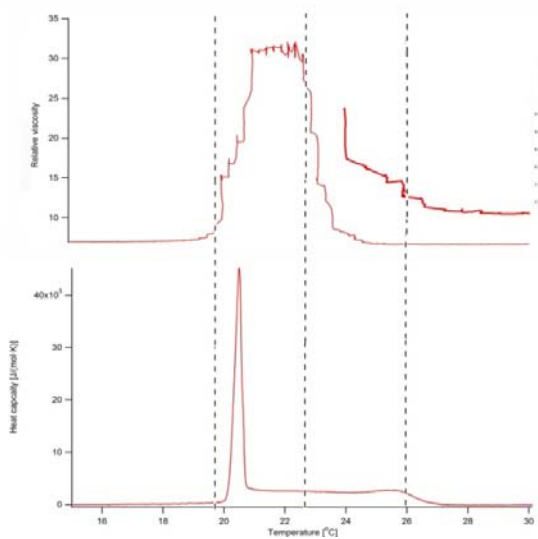


Figure 6.2: Viscosity and heat capacity curves for pH 11. Left viscosity axis is for the full viscosity curve. The right axis and the other curve shows a zoom of a part of the curve.

In accordance with previous work [3] the results showed connections between the viscosity and heat capacity curves:

- The first transition peak in the DSC coincides with the large increase in viscosity in the beginning of the high viscosity phase.
- The high viscosity region is situated between the two first peaks in the heat capacity curve
- The medium viscosity region begins after the second peak.
- The end of the phase transition for the heat capacity curve coincides with the end of the viscosity region where the viscosity is higher than constant value.

The heat capacity and viscosity curves have similar curve shape for pH 6. However the curves appear shifted in temperature for different regions of the curves. For instance for pH 6 the temperature region between the second and third peak does not coincide completely with the temperature region of the viscosity curve.

A few indications for the similar curve shape were possible: the first peak in the phase transition could be due to a structural transition to a more complicated structure such as the network formation, followed by a second peak indicating an initiation of stabilization the network followed by continuous network rearrangement. The third peak indicates a discontinuation of the network.

6.2 Vesicle sizes

6.2.1 Viscosity

From the viscosity curves there appears to be a very similar viscosity behavior for the different vesicle sizes above pH 7 (see figure 5.14-16 and A.1). According to figure A.3 there is a slight increase in viscosity at higher vesicle sizes. It can be seen in the figure that at pH below 7 the maximal value of the phase transition is very different when comparing the sonicated and extruded vesicles. This could indicate that either there is a difference between the two vesicle formation procedures, or that at low pH there occurs a different melting behavior where the curvature of the vesicles plays a role. According to the theory that there exist elongated structures would mean that the vesicle structure is preserved inside the phase transition. If this is true then the smaller vesicles should have higher viscosity because small vesicles have higher curvature. This effectively means that either it is very unlikely that the vesicle structure is preserved or that since the larger vesicles were extruded at a temperature higher than the phase transition they would change their properties before the initial viscosity and DSC measurements. As explained later the second reason is more unlikely.

6.2.2 DSC profiles

The DSC profiles showed very similar phase behavior for the different vesicle sizes and for the naturally dispersed DMPG solutions. It was therefore necessary to create area compressibility and bending modulus curves to study the phase behavior in more detail.

6.2.2.1 Area compressibility

For the different vesicle sizes it has been observed that the variation in the area compressibility in the phase transition is smaller than the variation for the naturally dispersed solution. This suggests that the naturally dispersed solution contains vesicles of all kind of sizes and that the melting behavior we see truly come from vesicles of similar size at different pH. Another interesting observation is that the main peak at the beginning of the phase transition narrows with increasing vesicle sizes. A possible reason for this could be that since the smaller vesicles have more curvature and are therefore more difficult to change in structure it would give a broader main peak if we assume that every heat capacity peak is related to a structural change. Also the presence of the second peak closer to the main peak at higher pH indicates that the structural changes associated with the second peak occur at a lower temperature at increasing ionic repulsion. Exactly what these structural changes are remains unknown. However another small possibility could be that the pH was not exactly precise or that the pH shifted due to the presence of the lipids, thus changing the peak.

6.2.2.2 Bending modulus

As explained previously the bending modulus reflects the change in the free energy with respect to the membrane curvature. The bending modulus is inversely related to the curvature of the system. [24] The bending modulus is extremely low throughout the entire phase transition. As can be observed in figure 5.20 the bending modulus is very low throughout the entire phase transition which indicates vesicles/structures carrying high curvature. Thus the curvature is of primary relevance, because the phase transition involves large changes in membrane curvature. [24] A problem with the bending modulus is that the model used is incomplete. DMPG has a complicated melting behavior and the reason for the incompleteness is that it most likely has two different bending moduli. The heat capacity profile shows an averaging of these two states.

In the phase transition the bending modulus decreases which gives an enhanced probability of lipid vesicles undergoing structural changes. This is necessary in order to decrease the elastic free energy to bend the membranes. [25] Bending the membranes is linked to an expansion of the outer monolayer and a compression of the inner monolayer which causes the heat capacity profiles to broaden. Such behavior would be in agreement with the theory involving vesicles that are formed into elongated structures. The experiments are however in contradiction to this because the different vesicle sizes are supposed to have different curvatures (see viscosity section) but the heat capacity does not broaden for the smaller vesicle sizes.

There can be two possible reasons for this behavior: as mentioned before it could be due to the change in properties of the vesicles after the sonication and extrusion and before they reach the phase transition. The variance in area compressibilities for the different vesicles does not support this assumption (see previous section). The other reason is more likely and states that since both the DSC and viscosity curves are (almost) the same for pH ≥ 6 then that is an indication that the

samples are the same which is in agreement with a kind of network formation. In this case the vesicle sizes are without significance or it may be possible that the area compressibility mentioned earlier for the main and second peak involves changes of the different vesicles into a specific network structure. However if no fusion between vesicles takes place one would expect different behavior for the different vesicle preparations. The network formation thus indicates that the vesicles fuse into the same type of network for the different vesicle sizes and thereby show the same thermal behavior.

6.3 Fluorescence microscopy

The images shown in section 5.5 are very interesting since they coincide with two theories. The giant vesicle in figure 5.20 could show a fractured vesicle with perforation within the phase transition which coincides with the theory proposed by Riske et al. On the other hand it may simply show the giant vesicle before it undergoes its structural transition. The network formation in figure 5.21 is the best example of the network formation to date and the structure resembles very much the structure obtained through electron microscopy [16]. Tubular structures can form when the sample has not completely equilibrated so it is unfortunately possible that the observed structures do not represent the typical phase behavior of DMPG.

Errors

The main errors appear to lie in the preparation of the samples, particularly the extrusion and evaporation procedure.

Extrusion produces populations of vesicles with sizes having a standard deviation lower than 10% about the mean diameter. This shows that the extrusion process is a reliable measure of obtaining the correct vesicles of interest. [23] The problem with extrusion is that the vesicles have to be made at 45°C and thereafter have to pass through the phase transition before any measurements can be made.

Creating giant vesicles using the evaporation procedure is relies on the fact that the lipids have to be dissolved in an organic solvent that gets evaporated. With this procedure some organic molecules are probably still attached to the membrane and could alter the vesicles properties. This might affect the phase behavior. The dyes influence on the phase transition (section A.3) could indicate that the dye has an influence on the structural transition which could complicate observing the phenomena. Different dye concentrations were used and it was only when the concentration of the dye was extremely low (1:3000 molar ratio) that the interesting structures appeared.

Another error could lie in the pH of the sample. Any deviation in pH can affect the phase behavior, particularly at low pH, and the pH of the sample can be affected by the addition of lipids.

The uncertainty for the baseline fitting is estimated to be around 10%. A problem with baseline fitting is that it is based on the person's judgment on where the transition is defined which affects both the end and starting points of the phase transition as well as the value of the phase transition.

Conclusion

The DSC, rheology and fluorescence results presented here, together with other features of the phase transition of low ionic strength below 100 mM can be explained by a network formation in the phase transition. As evidenced by the bending modulus curves this network should possess a softening of the membranes and a high average curvature throughout the entire phase transition. Such a network does not favor the sponge or bicontinuous phase, which have average curvature equal to zero, with segments having both positive and negative curvatures. This situation is also not favored by the repulsion between the polar headgroups. The model proposed by [17] corresponds to a network on the vesicle surface, having only positive excess curvature and seems conceptually the most likely change. The data collected here does not conclusively exclude either possibility but favors the formation of unilamellar vesicles with perforations that connect into a network.

The similar behavior of the DSC profiles as well as the similar magnitude of the viscosity curves at pH above 5 clearly indicate that the phase behavior is independent or at least only dependent in a small degree on the vesicles size. The area compressibility shows a smaller variance for the phase behavior at each vesicle size indicating that the vesicle structure is somehow retained throughout the phase transition. This further suggests that it is the network formation itself that contributes to the phase behavior. This suggests that no fusion occurs between the vesicles which clearly coincides with experimental findings and argues against the sponge network formation which favors fusion events.

Through the comparison of the heat capacity profiles with the viscosity indication of different structural transitions were possible. It suggests that a large structural transition occurs structural transition to a more complicated structure such as the network formation, followed by a second peak indicating an initiation of stabilization the network followed by continuous network rearrangement. The third peak indicates a discontinuation of the network. The fluorescence images support the formation of the network formation between unilamellar vesicles.

My experimental findings clearly support the notion that the phase behavior is dependent on charged headgroups throughout the phase transition. By varying the ionic strength and the pH it is clearly seen that the phase behavior changes. The peculiar phase behavior is only present at pH above 5 where the findings indicate that the charged headgroups are fully deprotonated and below 100 nM NaCl where the negative repulsion between the headgroups is not shielded. The lack of enthalpy change for the different phase transitions at different pH and salt concentration also indicate that a continuous acyl chain melting throughout the phase transition. I have also shown a pH dependence on the maximum of the viscosity. The increased viscosity coincides with the increase in pH, showing that the viscosity increases with the degree of dissociation which is proportional to the membrane potential.

References

1. Gerrit van Meer, Dennis R. Voelker and Gerald W. Feigensen. "Membrane lipids: where they are and how they behave." *Nature reviews molecular cell biology*. Vol. 9. (2008): 112-122.
2. Marie Domange Jordö. (2007). "The temperature dependence of the elasticity of giant lipid vesicles: An Optical Tweezers, Calorimetry and Confocal Microscopy study." Master Thesis.
3. Louise Revsbech Winther. (2008). "The Phase Transition of DMPG and its Dependence on pH." Bachelor Thesis.
4. Asger Tonnesen. (2008). "Electric Gradient Field Applied to Lipid Monolayers." Master Thesis.
5. Thomas Heimburg. (2007). Thermal Biophysics of Membranes. Wiley-Vch.
6. Kaare Græsbøll. (2008). "Influence of Anesthetics on the Nerve Membrane and the Nerve Pulse." Master Thesis.
7. Ching-hsien Huang and Shusen Li. (199). "Calorimetric and molecular mechanics studies of the thermotropic phase behavior of membrane phospholipids." *Biochimica et Acta*. 1422: 273-307.
8. Joan M. Boggs. "Lipid intermolecular hydrogen bonding - influence on structural organization and membrane function." *Biochimica Et Biophysica Acta*, 906 (1987): 353-404.
9. H. Träuble, M. Teubner, P. Woolley and H. Eibl. "Electrostatic interactions at charged lipid membranes. Effects of pH and univalent cations on membrane structure.". *Biophysical Chemistry*. 4, (Mar 1976): 319-342
10. R. Borsali., R. Pecora. (2008). "Soft-Matter Characterization." Springer.
11. Evan Evans. "Physical Properties of Surfactant Membranes: Thermal Transitions, Elasticity, Rigidity, Cohesion, and Colloidal Interactions." *Journal of Physical Chemistry*. Vol. 91. (1987): 4219-4228.
12. T. Heimburg. "Mechanical aspects of membrane thermodynamics. Estimation of the mechanical properties of lipid membranes close to the chain melting transition from calorimetry." *Biochimica Et Biophysica Acta*. 1415. (1998): 147-162.
13. Derek Marsh. "Elastic curvature constants of lipid monolayers and bilayers." *Chemistry and Physics of Lipids*. 144. (2006): 146-159.
14. Riske, KA, HG Dobereiner, and MT Lamy-Freund. "Gel-fluid transition in dilute versus concentrated DMPG aqueous dispersions." *Journal Of Physical Chemistry B*. Vol. 106 (2). (Jan 2002): 239-246.

15. Lamy-Freund, M. "The peculiar thermo-structural behavior of the anionic lipid DMPG." *Chemistry and Physics of Lipids* Vol. 122 (1-2). (Jan 2003): 19-32.
16. Matthias F. Schneider, Derek Marsh, Wolfgang Jahn, Beate Kloesgen and Thomas Heimburg. "Network formation of lipid membranes: Triggering structural transition by chain melting." *PNAS*. 96(25). (1997): 14312-14317.
17. Riske, K, L Amaral, H Dobereiner, and M Lamy. "Mesoscopic Structure in the Chain-Melting Regime of Anionic Phospholipid Vesicles: DMPG." *Biophysical Journal*, Vol. 86, (Jun 2004): 3722-3733.
18. R. Fernandez, K Riske, L Amaral, R Itri, and M Lamy. "Influence of salt on the structure of DMPG studied by SAXS and optical microscopy." *Biochimica Et Biophysica Acta-Biomembranes*, (Jul 2007): 907-916.
19. Alakoskela, Juha-Matti I, and Paavo K. J. Kinnunen. "Thermal phase behavior of DMPG: The exclusion of continuous network and dense aggregates." *Langmuir* Vol. 23 (8), (Mar 2007): 4203-4213.
20. K. Riske, Mário J. Politi, Wayne F. Reed and M. Teresa Lamy-Freund. "Temperature and ionic strength dependent light scattering of DMPG dispersions." *Chemistry and Physics of Lipids*. Vol 89. (1997): 31-44.
21. Riske, K, H Dobereiner, and M Lamy-Freund. "Comment on" Gel-Fluid Transition in Dilute versus Concentrated DMPG Aqueous Dispersions". " *Journal Of Physical Chemistry B*, Vol. 107. (Jan 2003): 5391-5392.
22. Alexander Moscho, Owe Orwar, Daniel T. Chu, Brien P. Modi and Richard N. Zare. "Rapid preparation of giant unilamellar vesicles." *PNAS*. Vol. 93 (1996): 11443-11447.
23. Bruylants, G, J Wouters, and C Michaux. "Differential scanning calorimetry in life science: thermodynamics, stability, molecular recognition and application in drug design." *Current medicinal chemistry* (Bentham Science Publishers) Vol. 12 (17). (2005): 2011-2020.
24. R. Rodríguez-García, L. R. Arriga, M. Mell, L. H. Molerio, I. López-Montero and F. Monroy. "Bimodal Spectrum for the curvature Fluctuations of Bilayer Vesicles: Pure Bending plus Hybrid Curvature-Dilation Modes." *Physical Review Letters*. 102. (2009): 128101
25. Vesselka P. Ivanova and Thomas Heimburg. "Histogram method to obtain heat capacities in lipid monolayers, curved bilayers, and membranes containing peptides." *Physical Review E*. 63. (2001): 041914.

Appendix A

A.1 Enthalpy change for phase transition

Enthalpy values for the phase transition were obtained using the same macro in IgorPro. From these ΔH were plotted for each NaCl concentration and different vesicle sizes within the pH 4-11 range. It has been demonstrated for DMPG [] that the enthalpy values depend highly on the baseline fitting. Even small variations in fitting parameters (setting a start and end of the transition values) can change enthalpy values up to 10%.

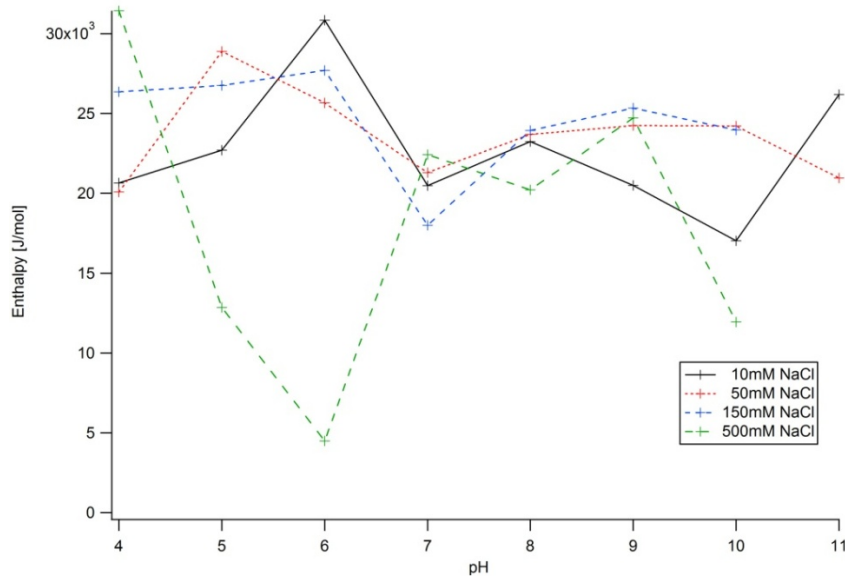


Figure A.1: Values for ΔH for the phase transition at different pH. Each line represents different NaCl concentrations.

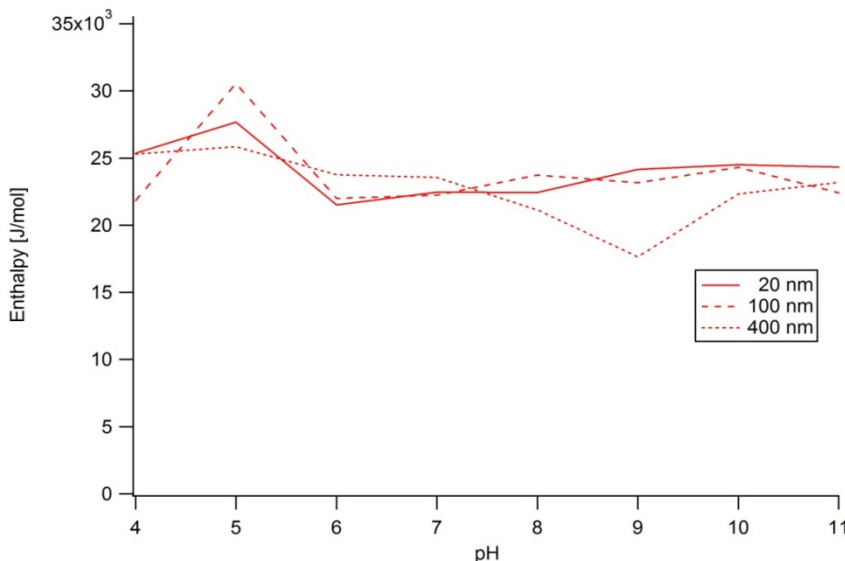


Figure A.2: Values for ΔH for the phase transition at different pH. Each line represents different vesicle sizes.

Figure A.1 shows for the different NaCl concentration that the enthalpy change from the transition does not vary too much for the different pH under different NaCl conditions. It also shows that the

different NaCl concentrations have approximately the same slope and height in their line-fit. This is however not true for 500 mM NaCl because some of the samples were partially degraded (pH 6 and pH 10) and it proved exceedingly difficult to avoid degradation at high salt concentration. The degradation causes the main transition to show a lower melting enthalpy.

Figure A.2 shows that the enthalpy change for the different vesicle sizes is very small (especially compared to the enthalpy change for the different NaCl concentrations). This indicates that the different vesicle sizes undergo the same phase behavior.

A.2 Highest viscosity change

The maximal values for the phase transition were plotted for the different vesicle sizes within the pH 4-11 range.

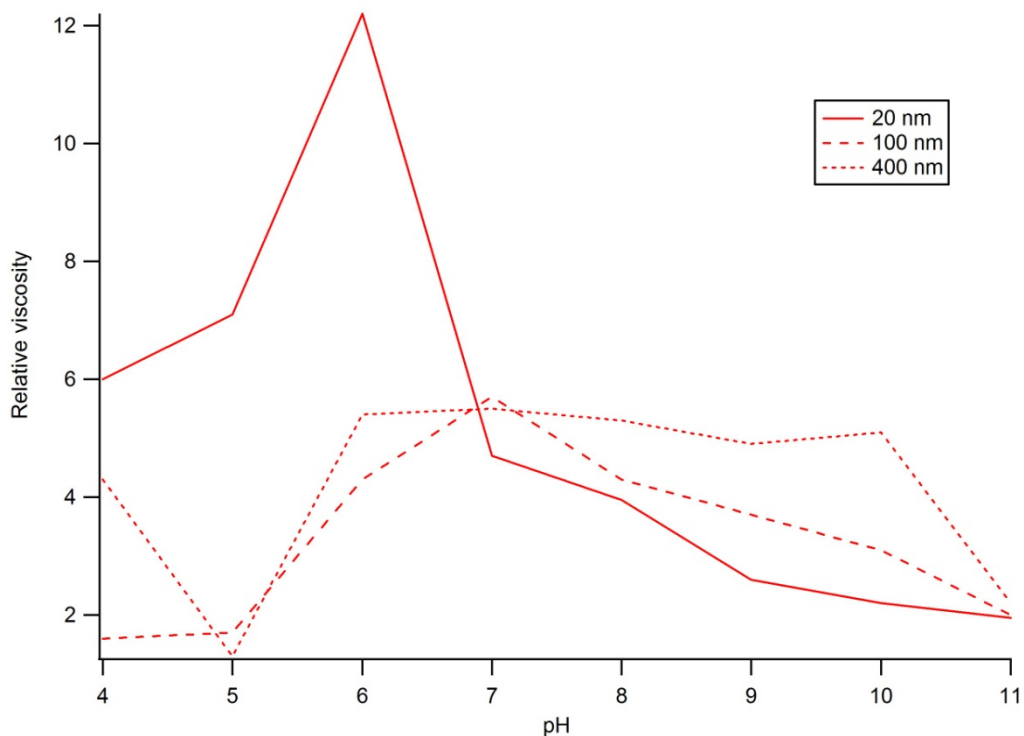


Figure A.3: Maximal values of high viscosity region within a pH range of 4-11. Each line represents different Vesicle sizes.

Figure A.3 shows a small increase in the viscosity at increasing vesicle size for pH ≥ 7 .

A.3 Influence of Dye

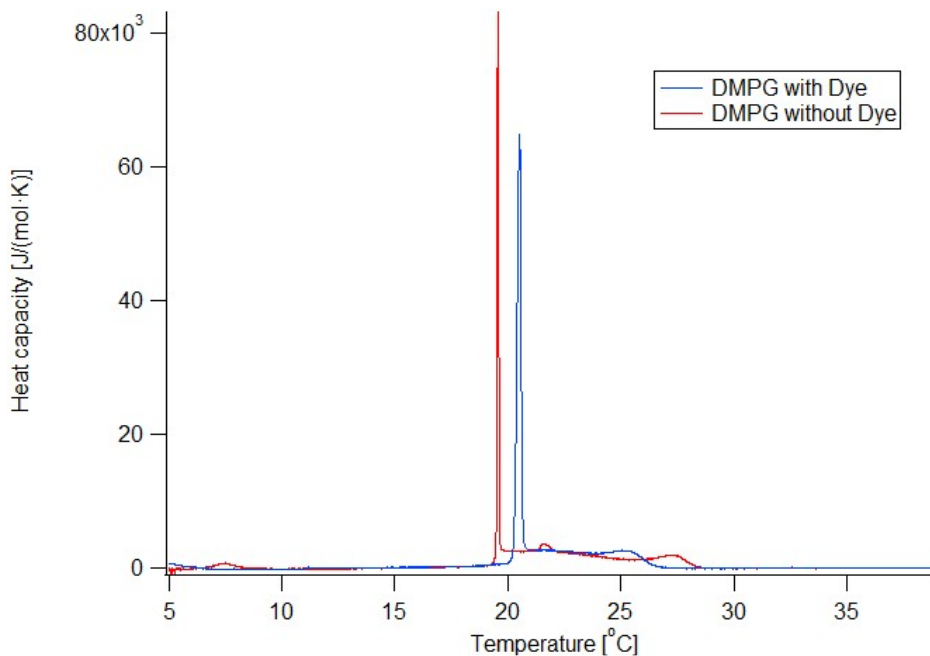


Figure 5.6: Heat capacity profile of DMPG with (blue) and without (red) 7mM dye at 10mM NaCl at pH 7.

Heat capacity profiles for DMPG with 7 μM DiI dye at pH 7 using 3 scans were obtained. By comparing heat capacity profiles of DMPG with/without dye the same pattern emerged: the phase transition appears shifted a little toward higher temperature.